

CLEARED FOR PUBLIC RELEASE

PL/PH 16 DEC 96

Sensor and Simulation Notes
Note 186
October, 1973

Admittances and Fields of a Planar Array
With Sources Excited in a Plane Wave Sequence*

Tom K. Liu

Dikewood Corporation, Westwood Research Branch
Los Angeles, California

Abstract

The admittances and fields of a planar array with the sources excited in a constant-amplitude, progressive-phase manner are derived and evaluated. The array consists of infinitely long wires, with each wire containing uniformly-spaced voltage sources. It is demonstrated that the propagating wave contains many lobes, each being a TEM plane wave propagating in a direction dependent on the frequency. The radiation field has non-vanishing low frequency components

* This work was supported in part by the Summa Foundation.

01-96-1900

I. Introduction

The sources of some EMP simulators are often in the form of pulser arrays [1], [2]. As pointed out by Baum [3], the series modules in these arrays are usually connected by conductors so that the radiated pulses contain the desired low frequency components. The sources of the array are excited in such a manner that at frequencies with wavelengths large compared to the module size, a plane wave is launched in a desired direction.

For a large array with many modules, the performance is close to that of an infinite array [4]. In this note, we consider an infinitely large planar array of infinitely long wires, with each wire containing uniformly spaced voltage sources. The geometry and the coordinate system are shown in Fig.1. MacFarlane [5], Wait [6] and Wright [7] have treated the scattering problem of the same geometry; some of their results share the same physical insight as the present problem. Baum [3] has obtained the very early time results for the far field. Here, the field of the array is expressed in terms of a set of E-type modes [8]. With this representation, it is possible to evaluate the current and the field components everywhere. The result clearly shows that at low frequencies, there is a TEM plane wave propagating in the desired direction, dictated by the phasing of the sources. The magnitude of this plane wave does not deteriorate with the distance from the source plane.

The formulation will be detailed in Section II. In Section III, we examine the expressions for the fields, calculating their scanning properties and magnitudes and phases. The driving-point admittances and the surface admittances are presented in Section IV.

II. Formulation

We start the formulation with the Pocklington's equation in the ζ -domain, where ζ is the Fourier transform variable of the coordinate z . The multiple sources and the plane wave sequence excitation are taken into account. The current and the vector potential contain a series of delta functions in ζ . This series, in performing the inverse Fourier transform, enables explicit expressions to be obtained in the space-domain. A Poisson summation formula is then applied and the resultant expressions are in the space harmonic form. Throughout this note, the time factor $e^{-i\omega t}$ is used.

The planar array, as shown in Fig.1, contains a two-dimensional periodic structure. The linear antennas are separated by a distance b , whereas the sources along an antenna are separated by a spacing d . We choose a source point as the origin of the coordinate system, and we designate the m -th antenna as the antenna that is at a distance $y = mb$ from the origin. The source on the m -th antenna at a distance $z = nd$ is designated as the (m,n) -th source. Delta-gap sources are first assumed in the derivation, however, in Section IV, we present the results for finite gap sources so that the driving-point admittances remain finite.

The plane wave sequence excitation [3], which launches a TEM plane wave in a desired direction at low frequencies with wavelengths large compared with the module dimensions, b and d , is re-defined in the frequency-domain as phase delays among the sources. For the (m,n) -th source, which is located at $(0\hat{x}, m\hat{y}, n\hat{z})$, the phase delay with respect to the source at the origin is

$$\text{Phase delay} = \exp[ik\hat{r}_0 \cdot (m\hat{y} + n\hat{z})]$$

where k is the wave number of free space, \hat{r}_0 is the unit position vector in the desired radiation direction: $\theta = \theta_0$ and $\phi = \phi_0$. This above expression is re-written as:

$$\text{Phase delay} = \exp[i(m\beta_y + n\beta_z)] \tag{1}$$

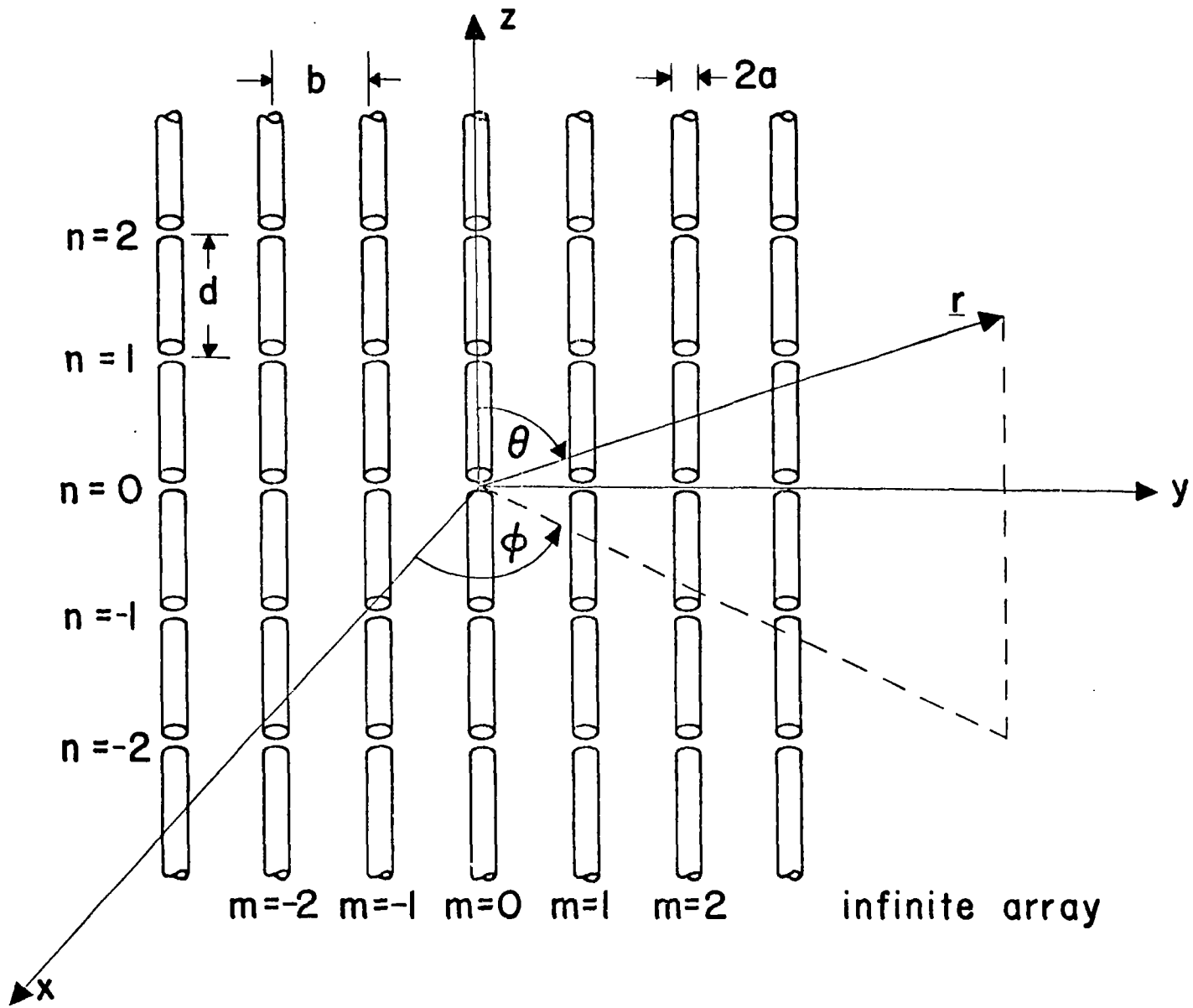


Fig.1. Geometry and coordinate system of the array.

where the incremental phase delay β_y in the y-direction is

$$\beta_y = k b \sin \theta_o \sin \phi_o \quad (2)$$

and the incremental phase delay β_z in the z-direction is

$$\beta_z = k d \cos \theta_o \quad (3)$$

For convenience, b is chosen to be the basic dimension and d is expressed in terms of b by the ratio

$$\eta = b/d \quad (4)$$

thus

$$\beta_z = \frac{1}{\eta} k b \cos \theta_o \quad (5)$$

For the special geometry, as shown in Fig.1 the Pocklington's integral equation [9] for the z-directed total current on the zero-th wire, I , is given by:

$$\left(\frac{\partial^2}{\partial z^2} + k^2 \right) \int_{-\infty}^{\infty} dz' \frac{I(z')}{2\pi a} \sum_{\ell=-\infty}^{\infty} e^{i\ell\beta_y} G_{\ell}(\underline{r};\underline{r}') = i\omega\epsilon_0 V \sum_{n=-\infty}^{\infty} \delta(z-nd) e^{in\beta_z} \quad (6)$$

where a is the radius of the wire, the voltages applied across the delta gaps are assumed to be of constant amplitude V , and $\delta(z)$ is the delta function. The function G_{ℓ} in (6), in general, is given by

$$G_{\ell}(\underline{r};\underline{r}') = \int_0^{2\pi} \frac{e^{ik|\underline{r}-\underline{r}'|}}{4\pi|\underline{r}-\underline{r}'|} a d\phi', \quad (7)$$

where both \underline{r} and \underline{r}' are on the surface of the ℓ -th and the zero-th wire, respectively. More specifically,

$$G_{\ell}(\underline{r};\underline{r}') = \int_0^{2\pi} \frac{e^{ik[(\ell b)^2 + (z-z')^2]^{\frac{1}{2}}}}{4\pi[(\ell b)^2 + (z-z')^2]^{\frac{1}{2}}} \text{ad}\phi'$$

for $\ell \neq 0$

(8)

$$G_0(\underline{r};\underline{r}') = \int_0^{2\pi} \frac{e^{ik[4a^2 \sin^2\{(\phi-\phi')/2\} + (z-z')^2]^{\frac{1}{2}}}}{4\pi[4a^2 \sin^2\{(\phi-\phi')/2\} + (z-z')^2]^{\frac{1}{2}}} \text{ad}\phi'$$

for $\ell = 0$

The following Fourier transform pair is defined:

$$\tilde{f}(\zeta) = \int_{-\infty}^{\infty} f(z) e^{-i\zeta z} dz$$

$$f(z) = \frac{1}{2\pi} \int_{-\infty}^{\infty} \tilde{f}(\zeta) e^{i\zeta z} d\zeta$$

(9)

It is observed that $G_{\ell}(\underline{r};\underline{r}')$ is a function of $z-z'$, and by the convolution theorem, Fourier transform of (6) becomes

$$(2\pi a)^{-1} (k^2 - \zeta^2)^{-\frac{1}{2}} \tilde{I}(\zeta) \sum_{\ell=-\infty}^{\infty} e^{i\ell\beta y} \tilde{G}_{\ell}(\zeta) = i\omega\epsilon_0 V \sum_{n=-\infty}^{\infty} e^{in(\beta_z - \zeta d)} \quad (10)$$

The Fourier transforms of (8) are readily found in [10]:

$$\tilde{G}_{\ell}(\zeta) = a K_0\left(|\ell|b \sqrt{\zeta^2 - k^2}\right), \quad \ell \neq 0 \quad (11)$$

and

$$\tilde{G}_0(\zeta) = a I_0(a\sqrt{\zeta^2-k^2}) K_0(a\sqrt{\zeta^2-k^2}), \quad \ell = 0 \quad (12)$$

where I_0 and K_0 are the modified Bessel functions of the first and the second kind, respectively, of order zero. From (10) to (12), we have

$$\tilde{I}(\zeta) = \frac{-i 2\pi\omega\epsilon_0 V \sum_{n=-\infty}^{\infty} e^{in(\beta_z - \zeta d)}}{(\zeta^2-k^2) \left[I_0(a\sqrt{\zeta^2-k^2}) K_0(a\sqrt{\zeta^2-k^2}) + \sum_{\ell \neq 0} e^{i\ell\beta_y} K_0(|\ell|b\sqrt{\zeta^2-k^2}) \right]} \quad (13)$$

The denominator deserves further study. We observe that

$$\frac{1}{(\zeta^2-k^2) I_0(a\sqrt{\zeta^2-k^2}) K_0(a\sqrt{\zeta^2-k^2})} = \frac{a}{(\zeta^2-k^2)^{\frac{1}{2}}} \left[\frac{I_1(a\sqrt{\zeta^2-k^2})}{I_0(a\sqrt{\zeta^2-k^2})} + \frac{K_1(a\sqrt{\zeta^2-k^2})}{K_0(a\sqrt{\zeta^2-k^2})} \right] \quad (14)$$

where I_1 and K_1 are the modified Bessel functions of the first and the second kind, respectively, of order one. As is inherent with the electric field formulation, the current $\tilde{I}(\zeta)$ in (13) contains two components: an external current (i.e., current on the outside wall of the wire), that contributes to radiation and an internal current (i.e., current on the inside wall of the wire), that contributes to the waveguide modes but not to radiation. Since we are interested in the radiation problem, the internal current should be left out* [10]. This corresponds to neglecting the first term in (14). The transformed current (external) now becomes

$$\tilde{I}(\zeta) = \frac{-i 2\pi\omega\epsilon_0 V K_1(a\sqrt{\zeta^2-k^2}) \sum_{n=-\infty}^{\infty} e^{in(\beta_z - \zeta d)}}{(\zeta^2-k^2)^{\frac{1}{2}} \left[K_0(a\sqrt{\zeta^2-k^2}) + I_0^{-1}(a\sqrt{\zeta^2-k^2}) \sum_{\ell \neq 0} e^{i\ell\beta_y} K_0(|\ell|b\sqrt{\zeta^2-k^2}) \right]} \quad (15)$$

Where the function $I_0^{-1}(z)$ is defined to be $1/I_0(z)$. The summation in the numerator can be converted into a summation of delta functions by applying the

*In the magnetic field formulation, one gets only one component of the current and does not have to make a choice.

Poisson's summation formula [11]:

$$\sum_{n=-\infty}^{\infty} f(n) = \sum_{q=-\infty}^{\infty} \int_{-\infty}^{\infty} f(n) e^{-i2\pi nq} dn \quad (16)$$

Therefore

$$\begin{aligned} \sum_{n=-\infty}^{\infty} e^{in(\beta_z - \zeta d)} &= \sum_{q=-\infty}^{\infty} \int_{-\infty}^{\infty} e^{in(\beta_z - \zeta d)} e^{-i2\pi nq} dn \\ &= \frac{2\pi}{d} \sum_{q=-\infty}^{\infty} \delta\left(\zeta - \frac{1}{d} (\beta_z - 2\pi q)\right) \end{aligned}$$

Equation (15) is now re-written as:

$$\tilde{I}(\zeta) = \frac{-i4\pi^2 a\omega\epsilon_0 V K_1(a\sqrt{\zeta^2 - k^2}) \sum_{q=-\infty}^{\infty} \delta(\zeta - (\beta_z - 2\pi q)/d)}{(\zeta^2 - k^2)^{1/2} d \left[K_0(a\sqrt{\zeta^2 - k^2}) + I_0^{-1}(a\sqrt{\zeta^2 - k^2}) \sum_{\ell \neq 0} e^{i\ell\beta_y} K_0(|\ell|b\sqrt{\zeta^2 - k^2}) \right]} \quad (17)$$

The delta function is non-zero at

$$\begin{aligned} \zeta &= (\beta_z - 2\pi q)/d. \\ &= k(\cos \theta_o - q\lambda/d) \end{aligned} \quad (18)$$

where λ is the wavelength corresponding to the wave number k . A new quantity κ_q is defined so that

$$\kappa_q = \cos \theta_o - q\lambda/d$$

From (5), we have

$$\kappa_q = \cos \theta_o - \eta q\lambda/b \quad (19)$$

The inverse Fourier transform of $\tilde{I}(\zeta)$, as defined by (10), can be readily evaluated using the integration property of the delta function,

$$\begin{aligned}
I(z) = \frac{-i2\pi aV}{Z_0 d} \sum_{q=-\infty}^{\infty} \left\{ K_1 \left(ka \sqrt{\kappa_q^2 - 1} \right) e^{ik\kappa_q z} \left[\left(\sqrt{\kappa_q^2 - 1} \right) \left\{ K_0 \left(ka \sqrt{\kappa_q^2 - 1} \right) \right. \right. \right. \\
\left. \left. \left. + I_0^{-1} \left(ka \sqrt{\kappa_q^2 - 1} \right) \sum_{\ell \neq 0} e^{i\ell\beta y} K_0 \left(k|\ell|b \sqrt{\kappa_q^2 - 1} \right) \right\} \right]^{-1} \right\} \quad (20)
\end{aligned}$$

where Z_0 is the wave impedance of free space. We now have an explicit expression for the current on the wires.

The field quantities can be conveniently expressed in terms of the magnetic vector potential, which will now be derived. The vector potential $\underline{A}(\underline{r})$ is parallel to the z-directed currents of the wires; hence

$$\underline{A}(\underline{r}) = A_z(\underline{r}) \hat{z}.$$

For an infinitely large array, we have

$$A_z(\underline{r}) = \mu_0 \sum_{m=-\infty}^{\infty} \int_{-\infty}^{\infty} dz' G_m(\underline{r}; \underline{r}') \cdot (2\pi a)^{-1} I_{(m)}(z')$$

where $I_{(m)}(z)$ is the z-directed current on the m-th wire, and G_m is given by (7), i.e.

$$G_m(\underline{r}; \underline{r}') = \int_0^{2\pi} \frac{e^{ik[x^2 + (y-mb)^2 + (z-z')^2]^{\frac{1}{2}}}}{4\pi[x^2 + (y-mb)^2 + (z-z')^2]^{\frac{1}{2}}} ad\phi' \quad (21)$$

The periodic nature of the structure requires

$$I_{(m)}(z) = I(z) e^{im\beta y}. \quad (22)$$

Hence

$$A_z(\underline{r}) = \mu_0 \int_{-\infty}^{\infty} dz' (2\pi a)^{-1} I(z') \sum_{m=-\infty}^{\infty} e^{im\beta y} G_m(\underline{r}; \underline{r}')$$

By the convolution theorem

$$\begin{aligned} \tilde{A}_z(\zeta) &= (2\pi a)^{-1} \mu_0 \tilde{I}(\zeta) \sum_{m=-\infty}^{\infty} e^{im\beta y} \tilde{G}_m(\zeta) \\ &= (2\pi)^{-1} \mu_0 \tilde{I}(\zeta) \sum_{m=-\infty}^{\infty} e^{im\beta y} K_0 \left([x^2 + (y - mb)^2]^{\frac{1}{2}} [\zeta^2 - k^2]^{\frac{1}{2}} \right) \end{aligned}$$

From (17)

$$\begin{aligned} \tilde{A}_z(\zeta) &= -i2\pi a \omega \mu_0 \varepsilon_0 V K_1 \left(a \sqrt{\zeta^2 - k^2} \right) \sum_{q=-\infty}^{\infty} \delta \left(\zeta - (\beta_z - 2\pi q) / d \right) \\ &\cdot \sum_{m=-\infty}^{\infty} e^{im\beta y} K_0 \left([x^2 + (y - mb)^2]^{\frac{1}{2}} [\zeta^2 - k^2]^{\frac{1}{2}} \right) \left\{ (\zeta^2 - k^2)^{\frac{1}{2}} d \left[K_0 \left(a \sqrt{\zeta^2 - k^2} \right) \right. \right. \\ &\left. \left. + I_0^{-1} \left(a \sqrt{\zeta^2 - k^2} \right) \sum_{\ell \neq 0} e^{i\ell\beta y} K_0 \left(|\ell| b \sqrt{\zeta^2 - k^2} \right) \right] \right\}^{-1} \end{aligned}$$

Again, utilizing the delta function integration property, the inverse Fourier transform becomes

$$\begin{aligned}
A_z(\underline{r}) = & \frac{-ia\omega\mu_0\varepsilon_0V}{kd} \sum_{q=-\infty}^{\infty} \left\{ K_1\left(ka\sqrt{\kappa_q^2 - 1}\right) e^{ik\kappa_q z} \right. \\
& \cdot \sum_{m=-\infty}^{\infty} e^{im\beta y} K_0\left(k[x^2+(y-mb)^2]^{\frac{1}{2}} [\kappa_q^2 - 1]^{\frac{1}{2}}\right) \left[(\kappa_q^2 - 1)^{\frac{1}{2}} \left\{ K_0\left(ka\sqrt{\kappa_q^2 - 1}\right) \right. \right. \\
& \left. \left. + I_0^{-1}\left(ka\sqrt{\kappa_q^2 - 1}\right) \sum_{\ell \neq 0} e^{i\ell\beta y} K_0\left(k|\ell|b\sqrt{\kappa_q^2 - 1}\right) \right\} \right]^{-1} \left. \right\} \quad (23)
\end{aligned}$$

We now apply the Poisson's summation formula to the m-series. From (16), we have

$$\begin{aligned}
& \sum_{m=-\infty}^{\infty} e^{im\beta y} K_0\left(k[x^2+(y-mb)^2]^{\frac{1}{2}} [\kappa_q^2 - 1]^{\frac{1}{2}}\right) \\
& = \sum_{p=-\infty}^{\infty} \int_{-\infty}^{\infty} dm e^{im\beta y} K_0\left(k[x^2+(y-mb)^2]^{\frac{1}{2}} [\kappa_q^2 - 1]^{\frac{1}{2}}\right) e^{-i2\pi mp}
\end{aligned}$$

The integral is evaluated with the aid of pair 868, Campbell and Foster [12].

Also from (2), we get

$$\sum_{m=-\infty}^{\infty} = \frac{\pi}{kb} \sum_{p=-\infty}^{\infty} \frac{e^{iky(\sin\theta_0 \sin\phi_0 - p\lambda/b)} e^{-kx[\kappa_q^2 + (\sin\theta_0 \sin\phi_0 - p\lambda/b)^2 - 1]^{\frac{1}{2}}}}{[\kappa_q^2 + (\sin\theta_0 \sin\phi_0 - p\lambda/b)^2 - 1]^{\frac{1}{2}}} \quad (24)$$

From (23) and (24), it is observed that if $A_z(\underline{r})$ is associated with a propagating wave, then the square roots in (24) must be negative imaginary. In parallel with (19) we define the following quantities

$$\kappa_p = \sin \theta_o \sin \phi_o - p\lambda/b \quad (25)$$

and

$$\kappa_{pq} = [1 - \kappa_p^2 - \kappa_q^2]^{1/2} \quad (26)$$

Equation (23) now becomes

$$A_z(\underline{r}) = \frac{\pi a_0 \mu_o \epsilon_o V}{k^2 b d} \sum_{p=-\infty}^{\infty} \sum_{q=-\infty}^{\infty} \left\{ K_1 \left(ka \sqrt{\kappa_q^2 - 1} \right) e^{ik[r_{pq}x + \kappa_p y + r_q z]} \right. \\ \left. \left[(r_q^2 - 1)^{1/2} \right\} K_0 \left(ka \sqrt{\kappa_q^2 - 1} \right) + I_0^{-1} \left(ka \sqrt{\kappa_q^2 - 1} \right) \right. \\ \left. \cdot \sum_{\ell \neq 0} e^{i\ell \beta y} K_0 \left(k|\ell|b \sqrt{\kappa_q^2 - 1} \right) \cdot r_{pq} \left\{ \right\}^{-1} \right\} \quad (27)$$

This expression is known to be in the space-harmonic form. We are now ready to express the field quantities through the following equations:

$$\underline{E} = -(i\omega\mu_0 \epsilon_0)^{-1} [\nabla(\nabla \cdot \underline{A}) + k^2 \underline{A}] \quad (28)$$

and

$$\underline{H} = \mu_0^{-1} \nabla \times \underline{A} \quad (29)$$

where

$$\underline{A}(\underline{r}) = A_z(\underline{r}) \hat{z}$$

Introducing a normalization factor $[V/(d \sin \theta_0)]^{-1}$ (the reason for using this value will be detailed in Section III), such that

$$\bar{E}(\underline{r}) = \underline{E}(\underline{r})/[V/(d \sin \theta_0)] \quad (30)$$

and

$$\bar{H}(\underline{r}) = Z_0 \underline{H}(\underline{r})/[V/(d \sin \theta_0)] \quad (31)$$

We now summarize all the expressions as follows:

$$\begin{aligned} \bar{E}_x &= \sum_{p=-\infty}^{\infty} \sum_{q=-\infty}^{\infty} F_q \kappa_q e^{i\mathbf{k}_{pq} \cdot \underline{r}} \\ \bar{E}_y &= \sum_{p=-\infty}^{\infty} \sum_{q=-\infty}^{\infty} F_q [\kappa_p \kappa_q / \kappa_{pq}] e^{i\mathbf{k}_{pq} \cdot \underline{r}} \\ \bar{E}_z &= - \sum_{p=-\infty}^{\infty} \sum_{q=-\infty}^{\infty} F_q [(1-\kappa_q^2) / \kappa_{pq}] e^{i\mathbf{k}_{pq} \cdot \underline{r}} \end{aligned} \quad (32)$$

$$\bar{H}_x = - \sum_{p=-\infty}^{\infty} \sum_{q=-\infty}^{\infty} F_q [\kappa_p / \kappa_{pq}] e^{i \mathbf{k}_{pq} \cdot \mathbf{r}}$$

$$\bar{H}_y = \sum_{p=-\infty}^{\infty} \sum_{q=-\infty}^{\infty} F_q e^{i \mathbf{k}_{pq} \cdot \mathbf{r}}$$

$$\bar{H}_z = 0 \quad (33)$$

$$I(z) = \frac{2\eta V}{z_o \sin \theta_o} \sum_{q=-\infty}^{\infty} F_q e^{i k \kappa_q z} \quad (34)$$

where

$$F_q = \frac{-i\pi \sin \theta_o}{\xi (\kappa_q^2 - 1)^{\frac{1}{2}}} \cdot \frac{K_1(ka \sqrt{\kappa_q^2 - 1})}{K_o(ka \sqrt{\kappa_q^2 - 1}) + I_o^{-1}(ka \sqrt{\kappa_q^2 - 1}) \sum_{\ell \neq 0} e^{i \ell \beta y} K_o(k|\ell|b \sqrt{\kappa_q^2 - 1})} \quad (35)$$

$$\frac{\mathbf{k}}{pq} = k(\kappa_{pq} \hat{x} + \kappa_{pq} \hat{y} + \kappa_q \hat{z})$$

$$\kappa_{pq} = [1 - \kappa_p^2 - \kappa_q^2]^{\frac{1}{2}}$$

$$\kappa_p = \sin \theta_o \sin \phi_o - p\lambda/b$$

$$\kappa_q = \cos \theta_o - \eta q \lambda / b \quad (36)$$

$$\eta = b/d$$

$$\xi = b/a \quad (37)$$

Equations (30) to (37) completely specify the performance of the array. In the following two sections, physical interpretation and numerical results will be given.

III. Fields

In this section, we point out that the expressions for the field quantities are associated with modes, and some properties of the modes are presented.

III.1 Orthogonality of the modes

The exponential factor in (32) and (33) can be shown to possess orthogonal properties over one module of the periodic structure. Let

$$\psi_{pq} = e^{\frac{ik}{-pq} \cdot \underline{r}} \quad (38)$$

Then, from (36), integrating over a module of the array gives

$$\begin{aligned} & \int_{z-d/2}^{z+d/2} \int_{y-b/2}^{y+b/2} \psi_{p_1 q_1} \psi_{p_2 q_2}^* dy dz \\ &= e^{ik(\kappa_{p_1 q_1} - \kappa_{p_2 q_2})x} \int_{z-d/2}^{z+d/2} dz e^{i2\pi(q_2 - q_1)z/d} \\ & \cdot \int_{y-b/2}^{y+b/2} dy e^{i2\pi(p_1 - p_2)y/d} \\ &= bd \delta_{p_1 p_2} \delta_{q_1 q_2} \end{aligned} \quad (39)$$

The factor ψ_{pq} is thus a mode function. The fields can now be written in the modal expressions.

$$\begin{aligned}\bar{\underline{E}} &= \sum_{p=-\infty}^{\infty} \sum_{q=-\infty}^{\infty} \bar{\underline{E}}_{pq} \\ \bar{\underline{H}} &= \sum_{p=-\infty}^{\infty} \sum_{q=-\infty}^{\infty} \bar{\underline{H}}_{pq}\end{aligned}\tag{40}$$

From (32), (33) and (40), $\bar{\underline{E}}_{pq}$ and $\bar{\underline{H}}_{pq}$ are easily identified in terms of the mode functions and the coefficients. It can be easily demonstrated that the fields $\bar{\underline{E}}_{pq}$ and $\bar{\underline{H}}_{pq}$ of each individual mode (p,q) satisfy Maxwell's equations.

From (33), it is observed that the H-field has no z-component. This type of modes, characterized by the vanishing of a magnetic field component parallel to the axial direction of a two-dimensional array, is called the E-type mode by Altschuler and Goldstone [8]. Sometimes, it is also called the longitudinal-section magnetic (LSM) mode [11].

III.2 Discussion of the field expressions

It can be easily verified that each mode behaves as a TEM wave, i.e.,

$$\underline{k}_{pq} \cdot \bar{\underline{E}}_{pq} = 0$$

and

$$\underline{k}_{pq} \cdot \bar{\underline{H}}_{pq} = 0$$

At a sufficiently large distance $|\underline{r}|$, some modes are greatly attenuated and constitute the evanescent waves. The propagating modes must have real κ_{pq} . From (36), this implies

$$\kappa_p^2 + \kappa_q^2 < 1\tag{41}$$

This further demands the following relationships:

$$|r_p| = |\sin \theta_o \sin \phi_o - p\lambda/b| < 1$$

$$|\kappa_q| = |\cos \theta_o - \eta q\lambda/b| < 1 \quad (42)$$

These expressions impose the condition that at very low frequency, i.e., very large λ , the only propagating mode is the (0,0) mode.

Another fact not observed in small arrays is that the magnitudes of the fields do not depend on the distance $|\underline{r}|$.

III.3 Direction and frequency span of the main beam

Mode (p,q) is associated with a propagation constant k_{pq} . Let this wave propagate in a direction $\theta = \theta_q$ and $\phi = \phi_{pq}$. Then, from (36)

$$\cos \theta_q = \kappa_q = \cos \theta_o - \eta q\lambda/b$$

$$\sin \theta_q \sin \phi_{pq} = \kappa_p = \sin \theta_o \sin \phi_o - p\lambda/b \quad (43)$$

It is clear that θ_q and ϕ_{pq} are functions of frequency for $q \neq 0$ and $p \neq 0$, respectively. This property is referred to as scanning. Each mode is associated with a single radiated beam in a specific direction. We call the (0,0) mode the main beam and all others the grating lobes [4].

The main beam corresponds to the (0,0) mode and is a propagating wave at all frequencies in the direction $\theta = \theta_o$ and $\phi = \phi_o$, as indicated in (43). This is the desired direction as defined by the plane-wave excitation sequence.

Of specific interest is the low frequency (and hence the late time) behavior of this main beam. As pointed out in (42), the (0,0) mode is the only propagating wave at low frequency and is of particular importance to EMP simulation.

The frequency span of the (0,0) mode, from 0 to c/λ_{pq}^c where c is the velocity of light, is the range within which only this mode is present. The quantity λ_{pq}^c is the cut-off wavelength of the second mode and can be obtained

from (36) by setting $\kappa_{pq} = 0$. This yields

$$b/\lambda_{pq}^c = \{[(p \sin \theta_o \sin \phi_o + \eta q \cos \theta_o)^2 + (p^2 + \eta^2 q^2) \sin^2 \theta_o \cos^2 \phi_o]^{1/2} - (p \sin \theta_o \sin \phi_o + \eta q \cos \theta_o)\} / [\sin^2 \theta_o \cos^2 \phi_o] \quad (44)$$

The second mode corresponds to the grating lobe with the smallest value of λ_{pq}^c . Let us restrict our investigation to the region

$$0^\circ \leq \theta_o \leq 90^\circ \quad \text{and} \quad 0^\circ \leq \phi_o \leq 90^\circ \quad (45)$$

For other regions, we would obtain results similar to the following because (44) shows definite symmetry in p , q , θ_o and ϕ_o for certain combinations of positive and negative values of these quantities. This is illustrated partially in Fig.2 and Fig.5. These figures are described in the following paragraphs.

With the condition (45), it is observed in (44) that the second mode is either (0,1) or (1,0), and

$$b/\lambda_{10}^c = (1 - \sin \phi_o) / [\sin \theta_o \cos^2 \phi_o]$$

$$b/\lambda_{01}^c = \eta [(1 - \sin^2 \theta_o \sin^2 \phi_o)^{1/2} - \cos \theta_o] / [\sin^2 \theta_o \cos^2 \phi_o] \quad (46)$$

In fact, there are break-off values of η , denoted by η_b , at which one mode takes over from the other as the second mode

$$\eta_b = \frac{\sin \theta_o (1 - \sin \phi_o)}{(1 - \sin^2 \theta_o \sin^2 \phi_o)^{1/2} - \cos \theta_o} \quad (47)$$

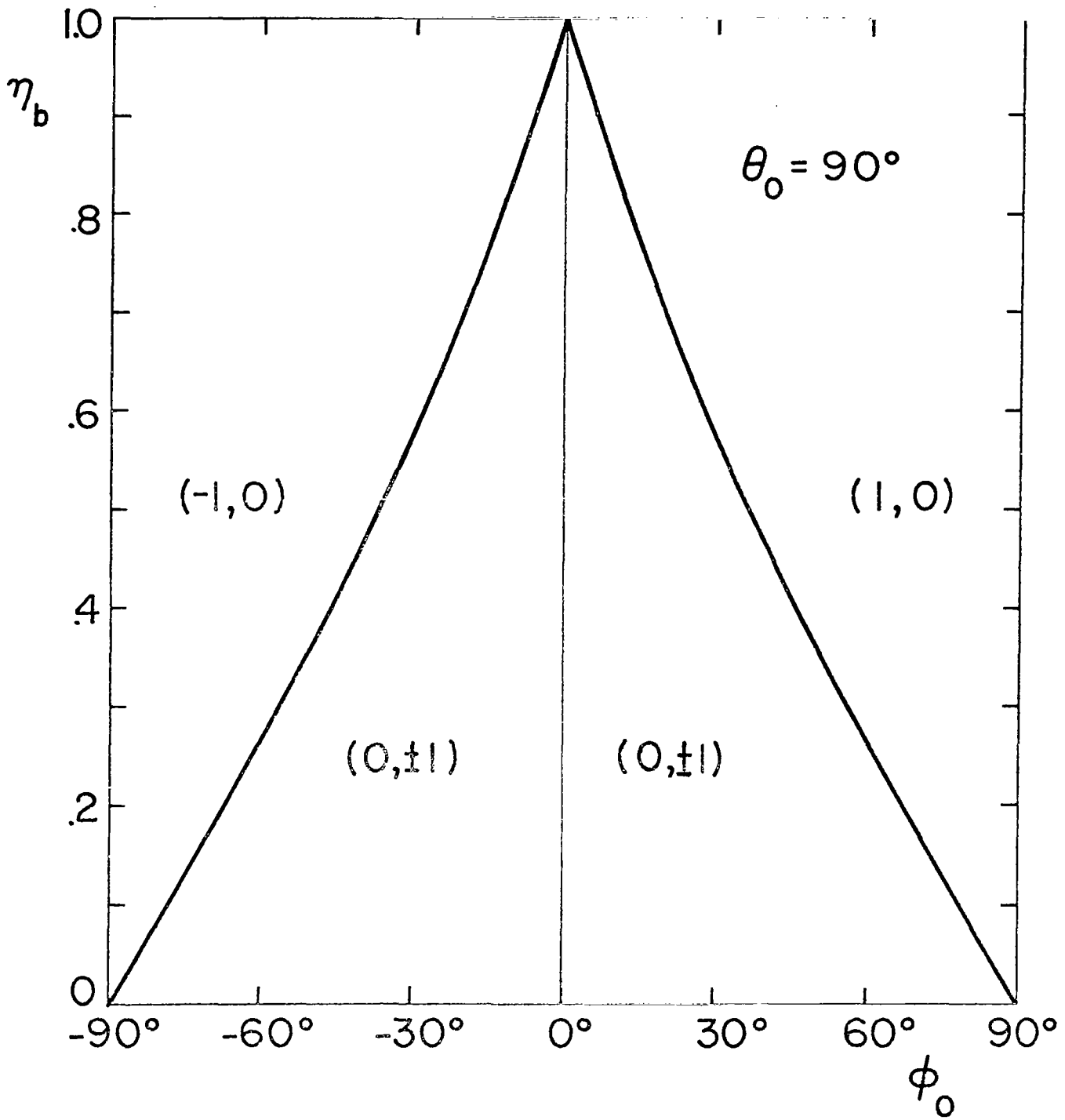


Fig.2. η_b versus ϕ_0 for $\theta_0 = 90^\circ$. η_b is the value b/d at which two modes change over to be the second propagating mode.

For $\theta_o = 90^\circ$, η_b is plotted as a function of ϕ_o in Fig.2. Above the curve, the (1,0) mode is the second mode, and below the curve, the (0,+1) modes. On the same figure, the corresponding case for $-90^\circ \leq \phi_o \leq 0^\circ$ is shown for the two modes (-1,0) and (0,-1). This serves to illustrate the symmetry nature of p, q, θ_o and ϕ_o . In Fig.3, the cut-off frequency of the second mode expressed as b/λ_{pq}^c , is plotted as a function of η with ϕ_o as a parameter. Again we set $\theta_o = 90^\circ$ in this case. The horizontal section is where the (1,0) mode is the second mode; and the sloped section, the (0,1) mode. The region under the (0,1) and (1,0) curves, for a particular ϕ_o , is where only the (0,0) mode propagates. In Fig.4, for the same θ_o , b/λ_{pq}^c of the second mode is plotted versus ϕ_o , with η being the parameter. In this graph, for a particular η , the region under the (0,1) and (1,0) curves is where only the (0,0) mode propagates.

We now present similar curves for the other principal plane $\phi_o = 0^\circ$. Figs.5 to 7 are in exact correspondence to Figs.2 to 4, respectively, with θ_o replacing ϕ_o as the parameter.

III.4 Frequency scanning of the grating lobes

Equations (43) indicate that the directions of the grating lobes are frequency dependent. From (36) and (43), the cut-off frequency of the (p,q) mode is given by the condition $\kappa_{pq} = 0$, which demands

$$\sin \theta_q \cos \phi_{pq} = 0$$

Restricting to the +x direction, this implies

$$\theta_q \Big|_{\text{cut-off}} = 0^\circ \text{ or } \phi_{pq} \Big|_{\text{cut-off}} = 90^\circ \quad (48)$$

This condition means that the grating lobes always start scanning in the source plane, either in the +z direction or the +y direction.

For very high frequency such that $p\lambda \approx 0$ and $q\lambda \approx 0$, we have

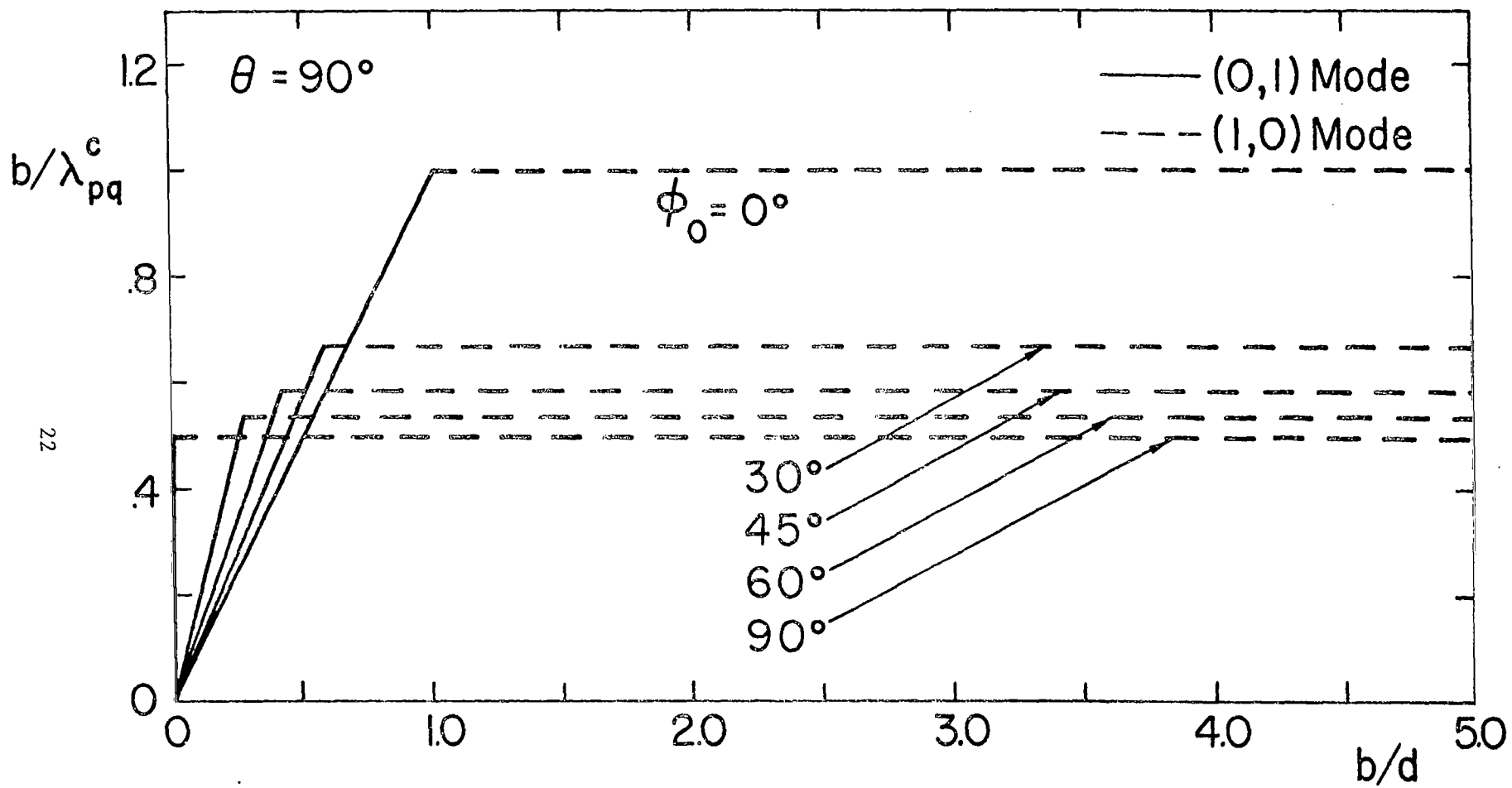


Fig.3. Cut-off frequency of the second propagating mode as a function of b/d for various angles of ϕ_0 . $\theta_0 = 90^\circ$.

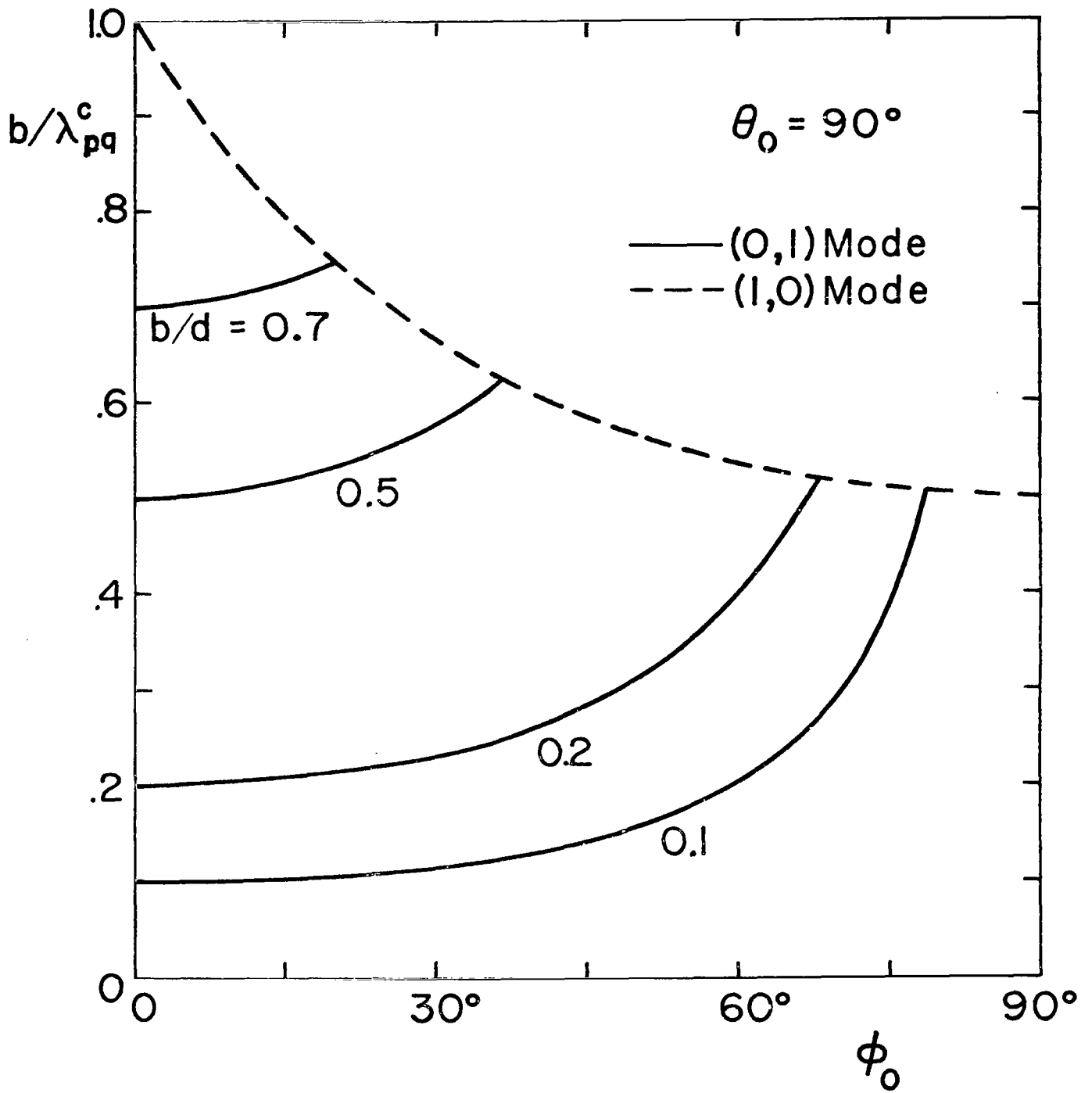


Fig.4. Cut-off frequency of the second propagating mode as a function of ϕ_0 for various values of b/d . $\theta_0 = 90^\circ$.

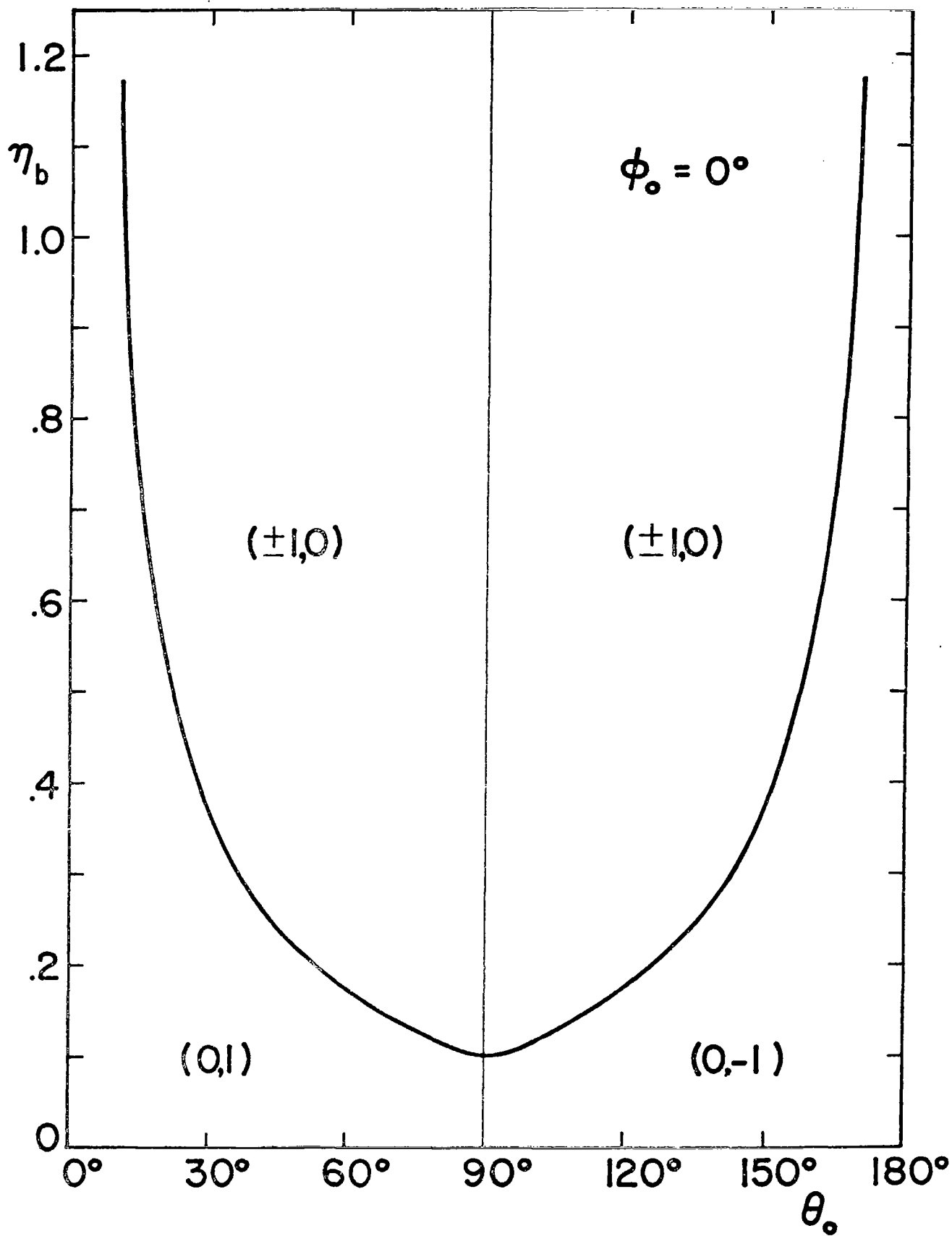


Fig.5. η_b versus θ_o for $\phi_o = 0^\circ$. η_b is the value b/d at which two modes change over to be the second propagating mode.

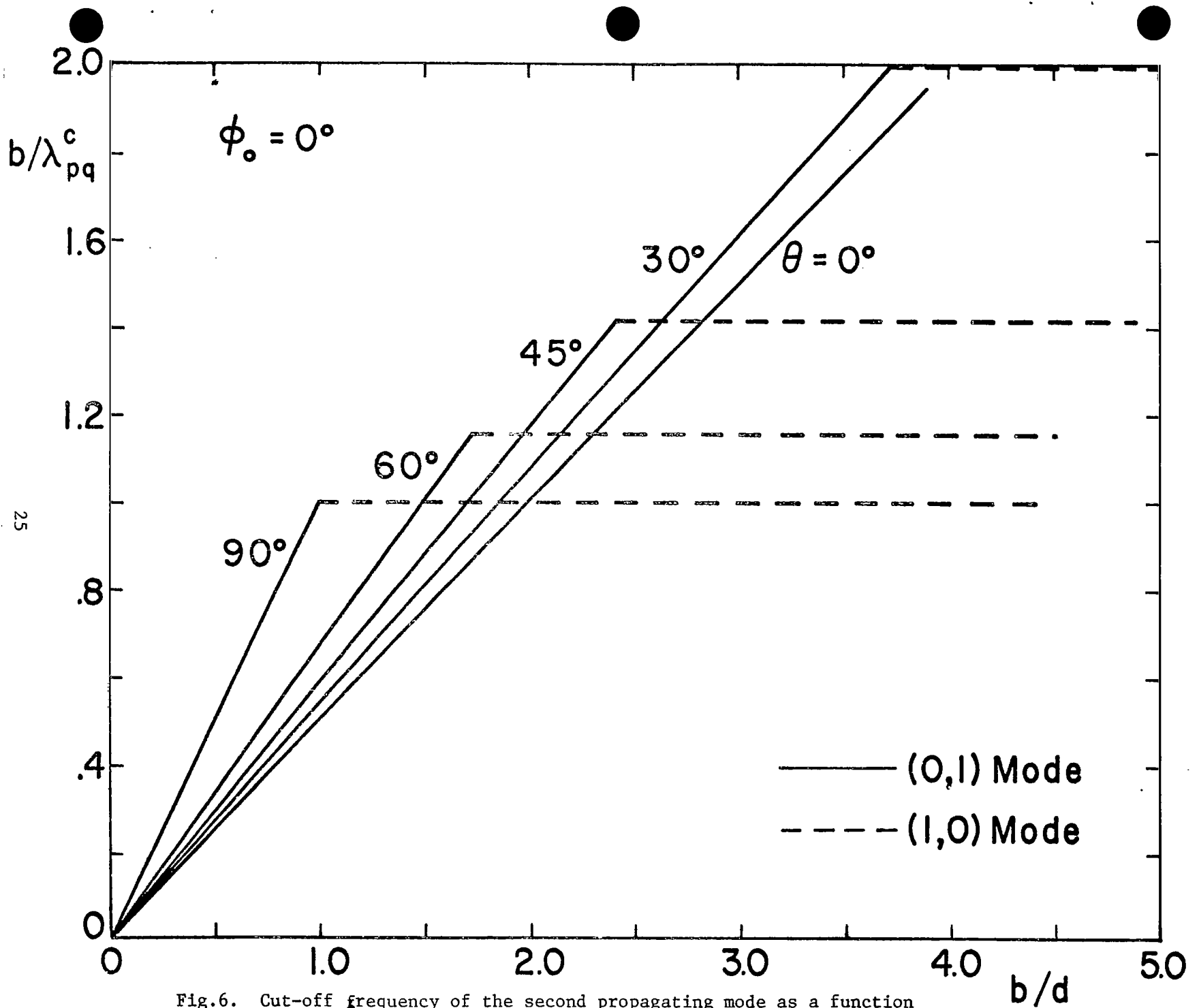


Fig.6. Cut-off frequency of the second propagating mode as a function of b/d for various angles of θ_0 . $\phi_0 = 0^\circ$.

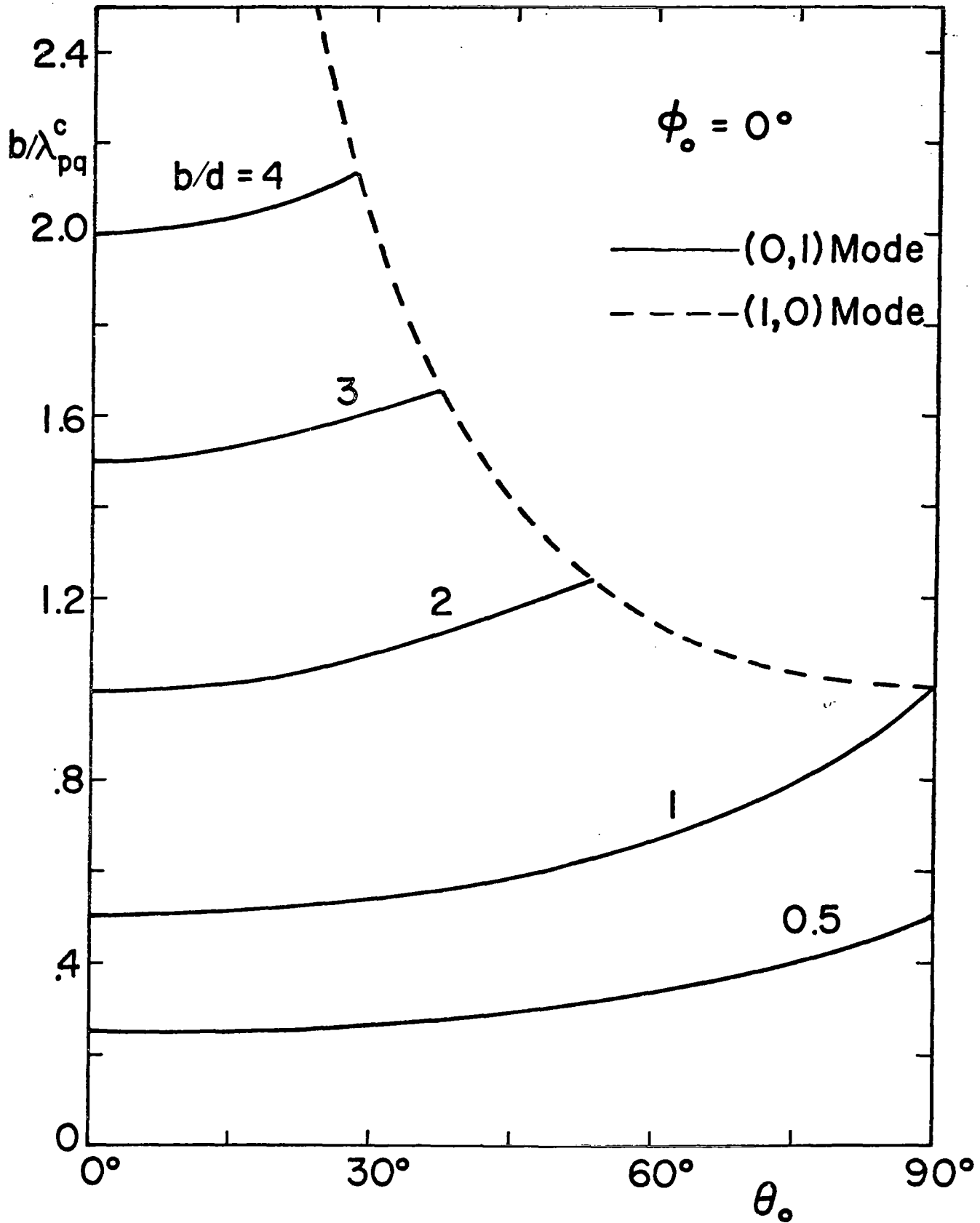


Fig.7. Cut-off frequency of the second propagating mode as a function of θ_0 for various values of b/d . $\phi_0 = 0^\circ$.

$$\theta_q|_{k \rightarrow \infty} \approx \theta_o \quad \text{and} \quad \phi_{pq}|_{k \rightarrow \infty} \approx \phi_o \quad (49)$$

i.e., the grating lobes propagate in the desired direction.

In Fig.8, we present the scanning of (0,1) and (1,0) modes as a function of frequency, in the form of b/λ . In this case, $\theta_o = 90^\circ$ and $\phi_o = 0^\circ$, with η as the parameter. The cut-off frequency directions and the high frequency directions are observed to behave as indicated by (48) and (49).

In Figs.9-12, we present the scanning for various values of θ_o and ϕ_o .

III.5 Field Magnitudes

We are now in the position to investigate the magnitudes of the fields of the propagating waves. It is found that the basic problem in the evaluation is to calculate the amplitude factor F_q . Of particular interest is the low frequency behavior of the field, which corresponds to the late time behavior of the simulated EMP.

For a particular geometry at a particular frequency, the number of propagating modes is first determined using (41) and (42). The total field is then obtained by the double sums in (32) and (33). The method of evaluating F_q is detailed in Appendix A.

The low frequency (and hence late time) behavior of the fields is of interest. As pointed out earlier, there is only the (0,0) mode that propagates at this frequency. Hence, from (32) and (36)

$$\begin{aligned} \bar{\mathbf{E}}|_{k \rightarrow 0} = F_o \{ & \cos \theta_o \hat{\mathbf{x}} + [(\sin \theta_o \sin \phi_o) \cos \theta_o / (\sin \theta_o \sin \phi_o)] \hat{\mathbf{y}} \\ & - [(\sin^2 \theta_o) / (\sin \theta_o \cos \phi_o)] \hat{\mathbf{z}} \} \cdot e^{\frac{ik}{pq} \cdot \mathbf{r}} \end{aligned}$$

and

$$|\bar{\mathbf{E}}|_{k \rightarrow 0} = |F_o| / \cos \phi_o$$

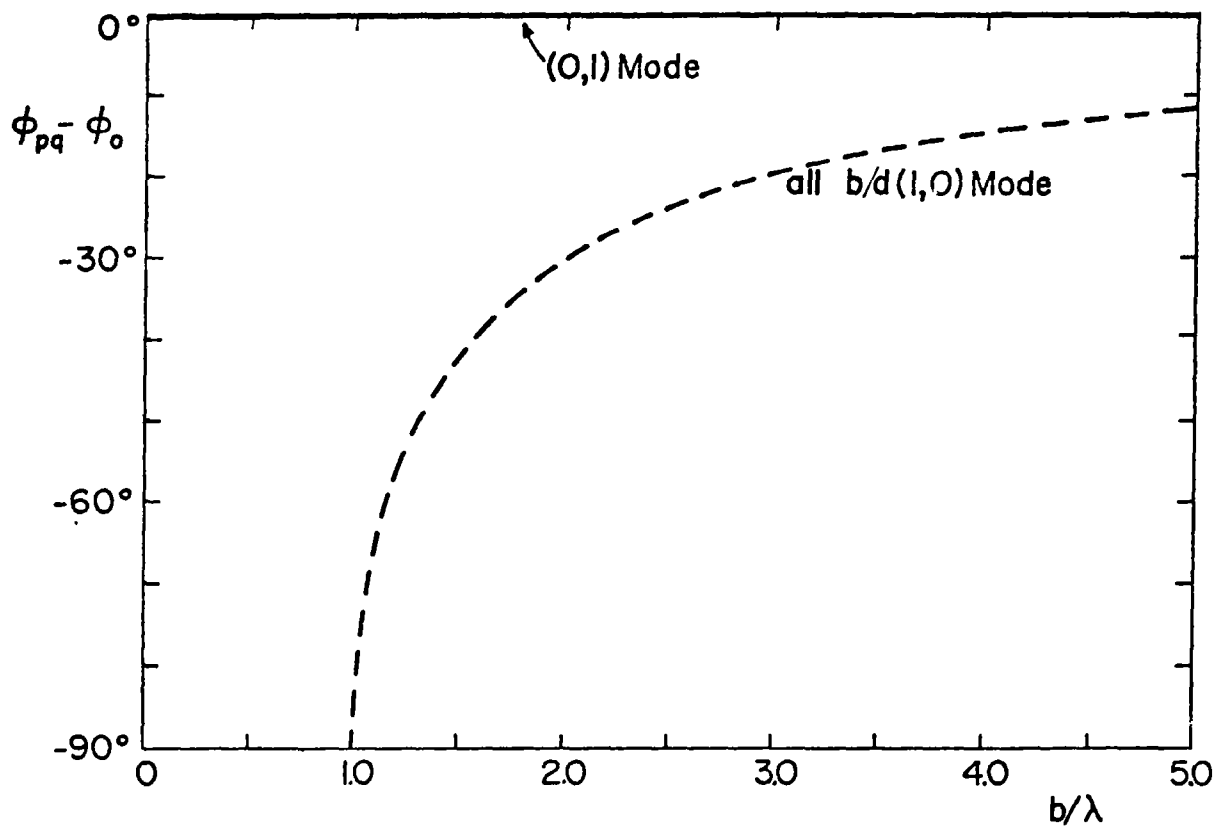
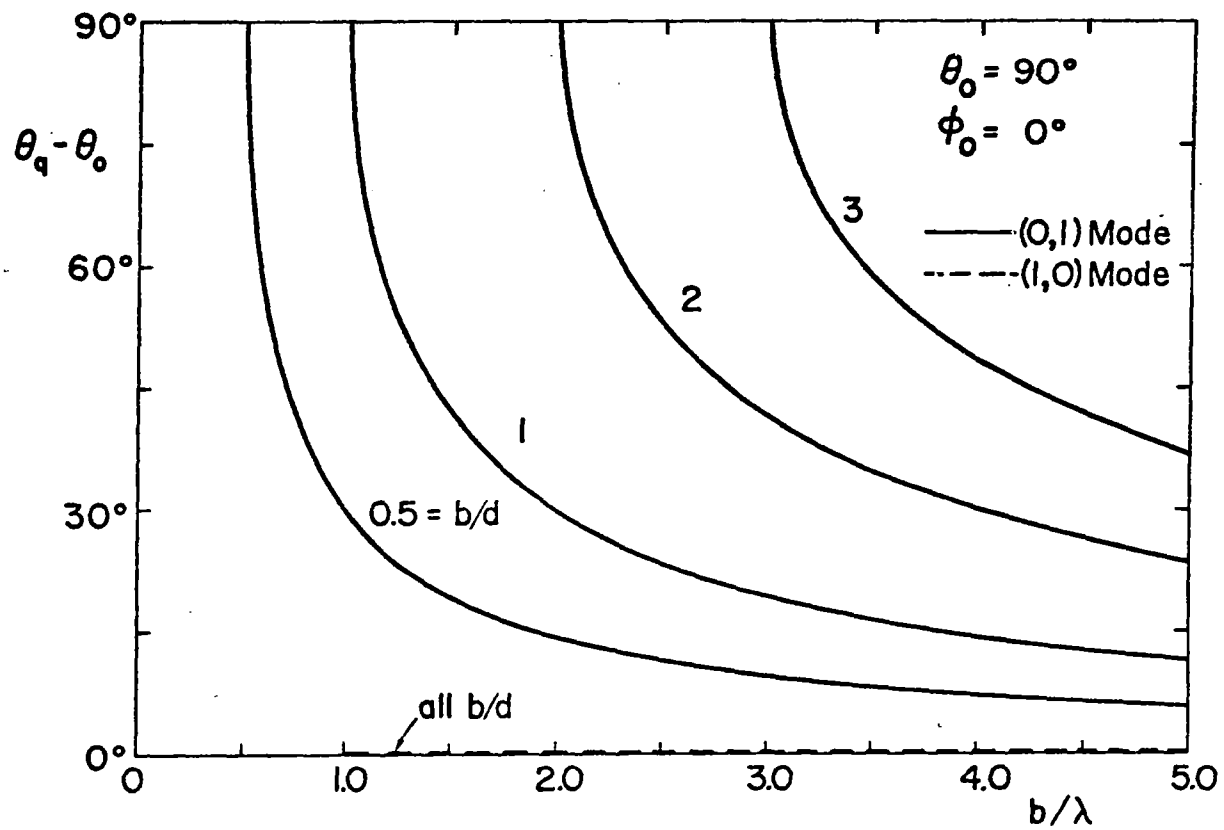


Fig.8. Frequency scanning of (0,1) and (1,0) mode for $\theta_0 = 90^\circ$, $\phi_0 = 0^\circ$.

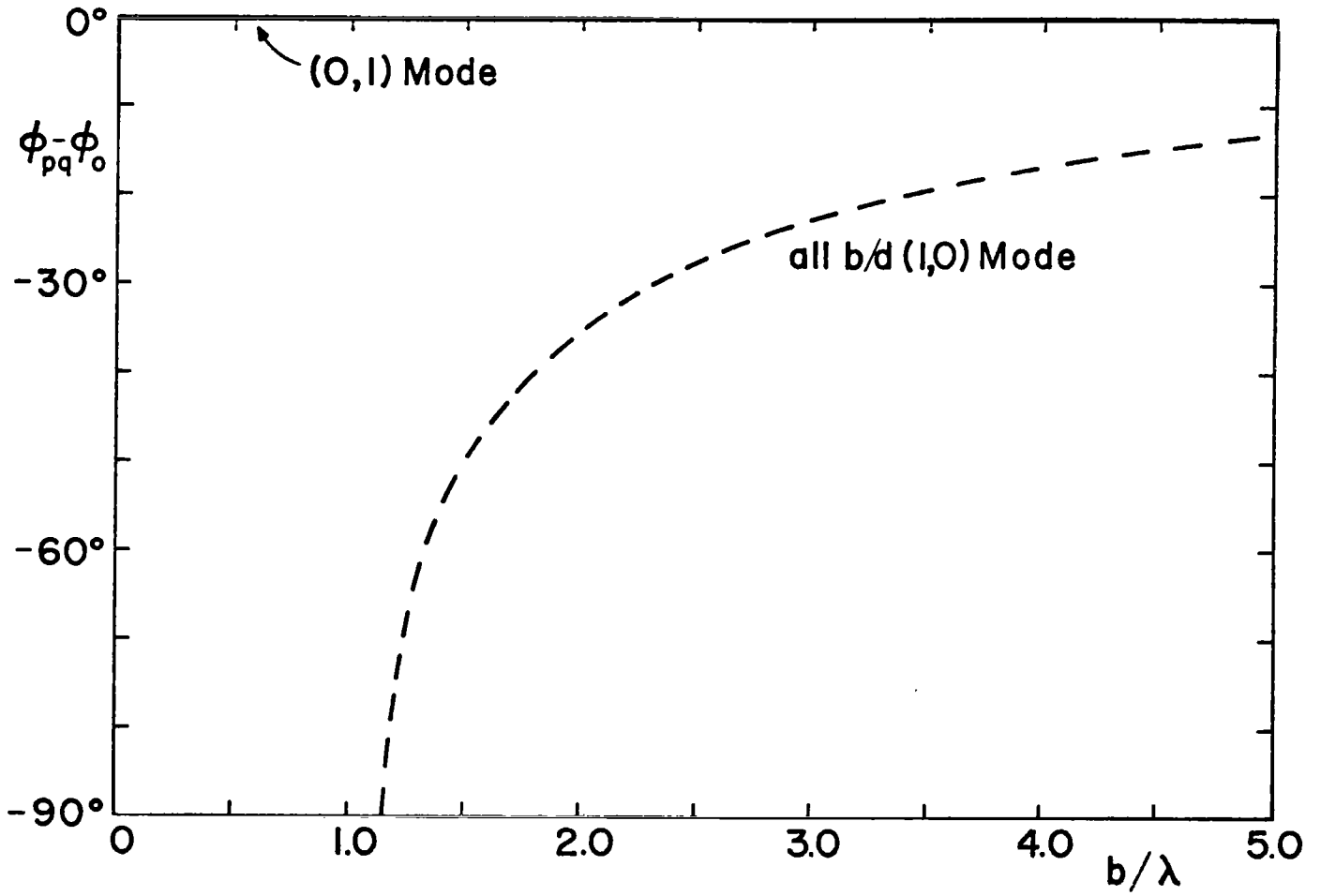
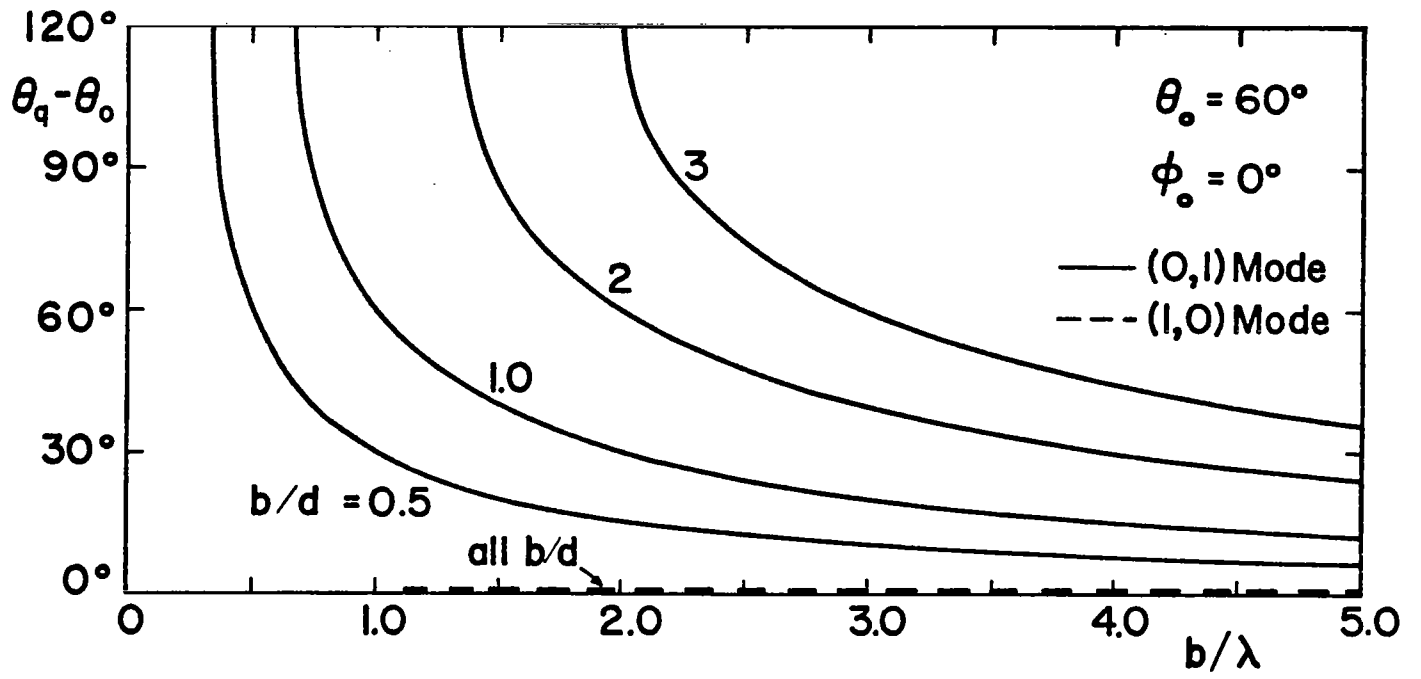


Fig.9. Frequency scanning of $(0,1)$ and $(1,0)$ mode for $\theta_0 = 60^\circ$, $\phi_0 = 0^\circ$.

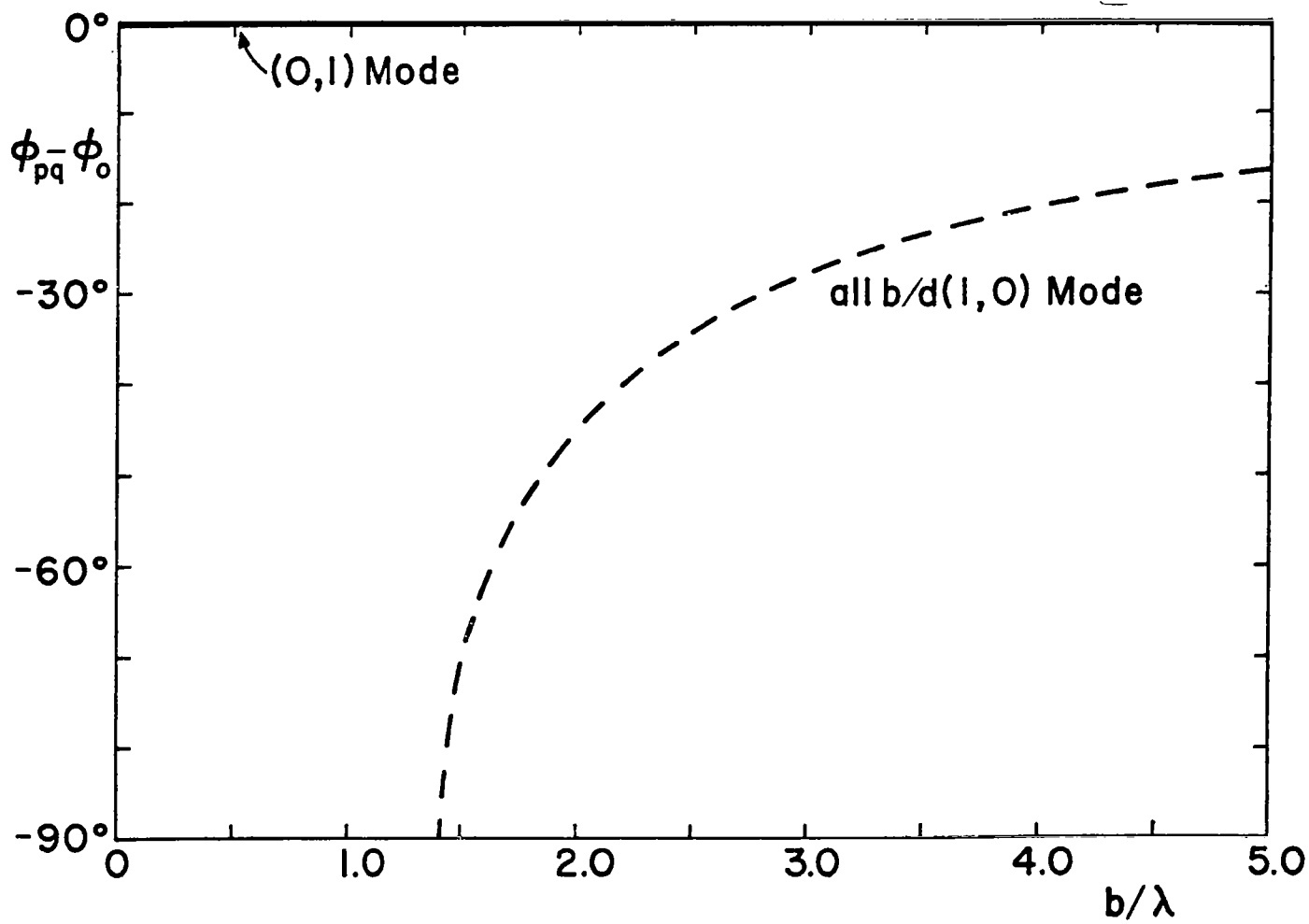
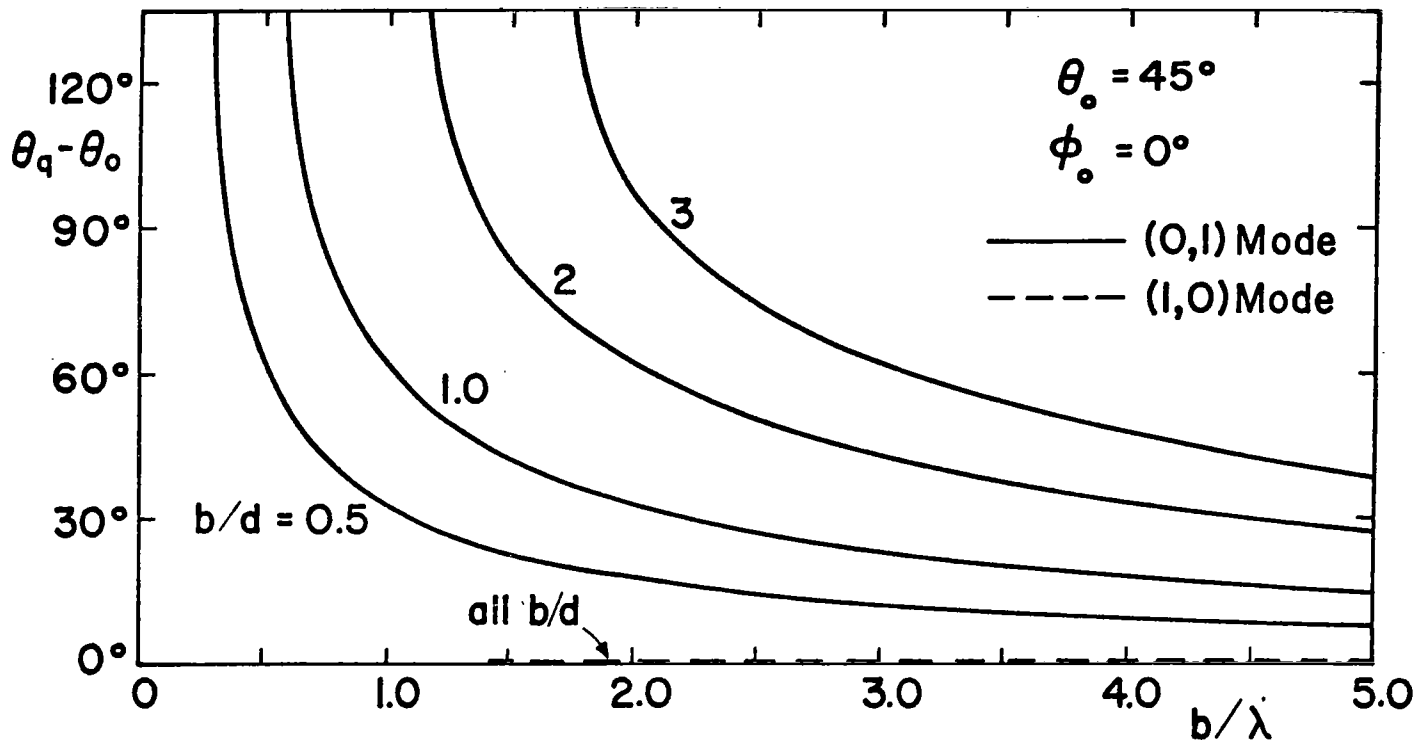


Fig.10. Frequency scanning of (0,1) and (1,0) mode for $\theta_0 = 45^\circ$, $\phi_0 = 0^\circ$.

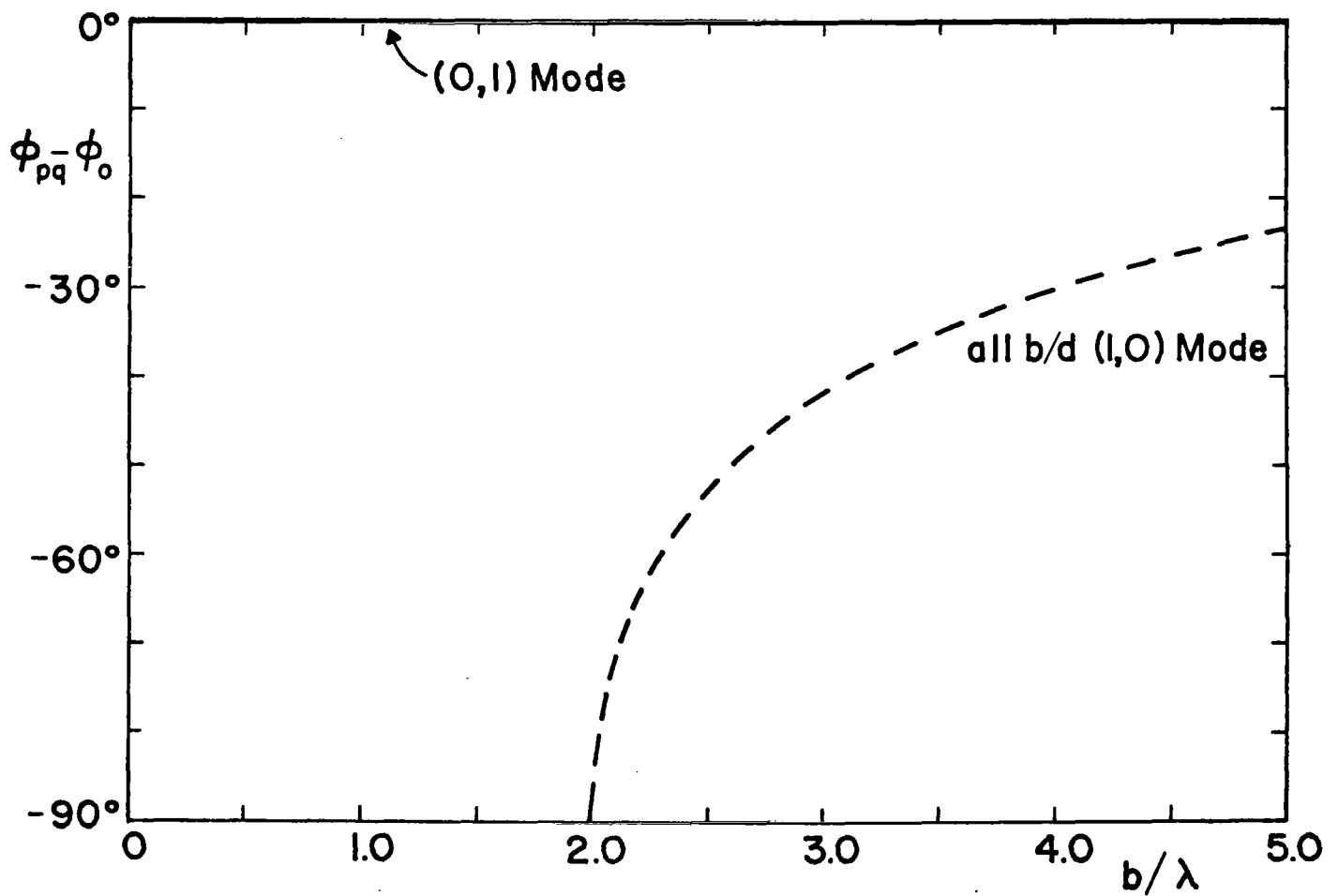
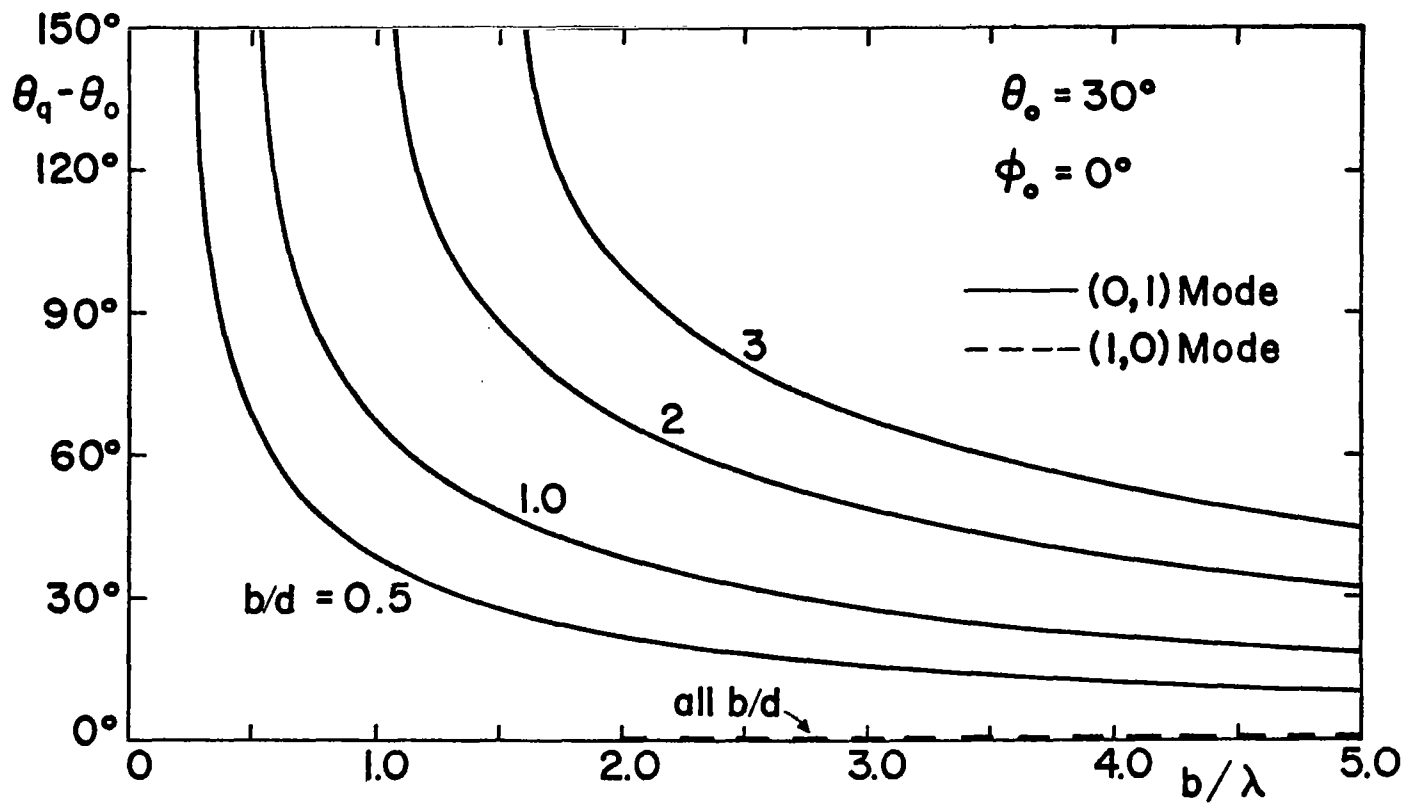


Fig.11. Frequency scanning of (0,1) and (1,0) mode for $\theta_0 = 30^\circ$, $\phi_0 = 0^\circ$.

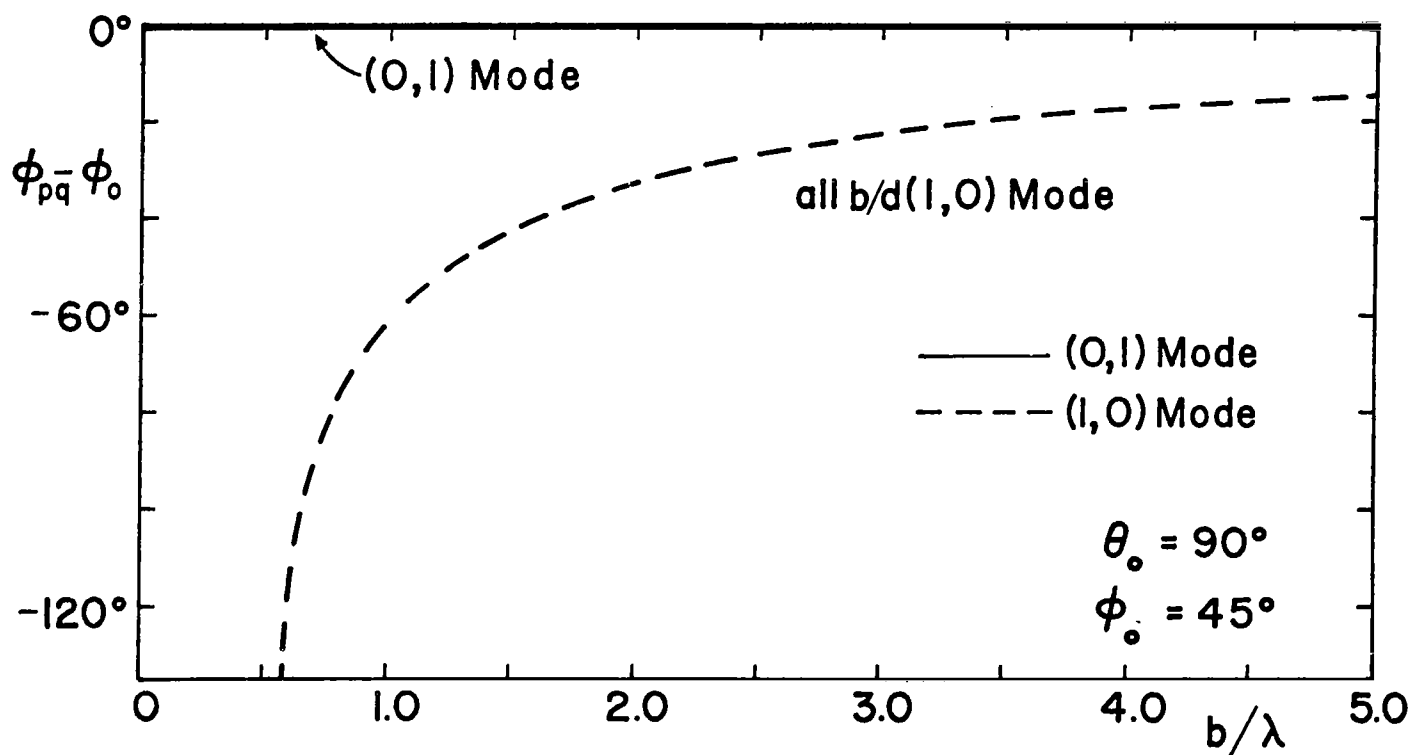
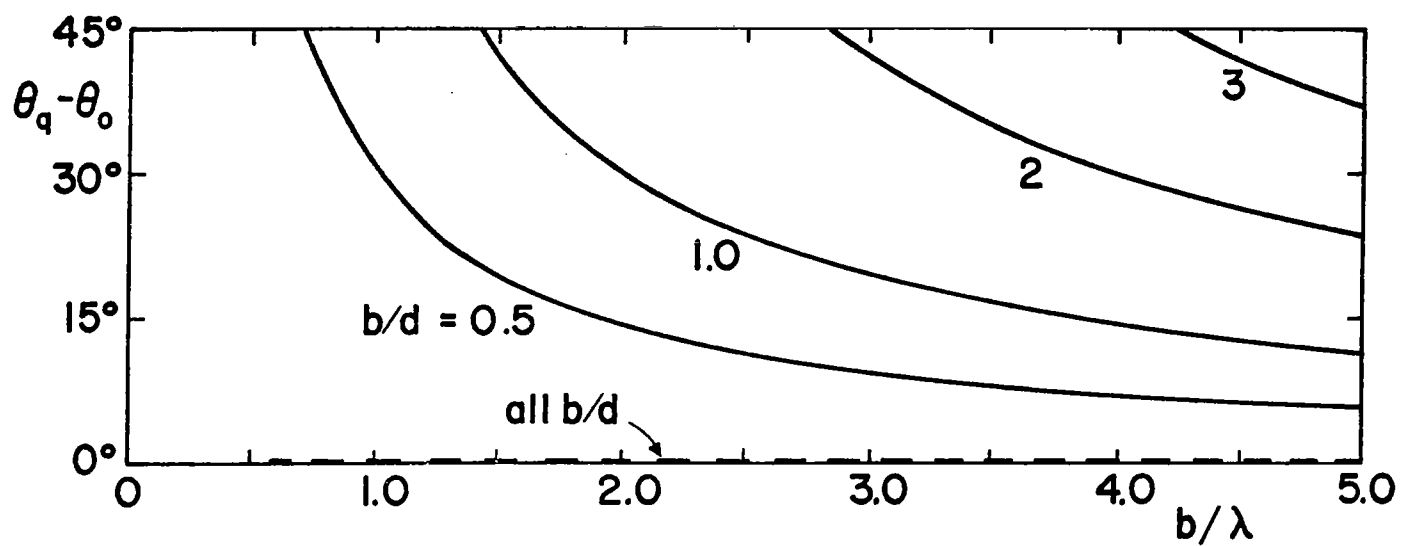


Fig.12. Frequency scanning of $(0,1)$ and $(1,0)$ mode for $\theta_0 = 90^\circ$, $\phi_0 = 45^\circ$.

From (A.7) of Appendix A, we get

$$|\overline{E}|_{k \rightarrow 0} = 1 \quad (50)$$

This gives the reason for choosing the normalization constant $V/(d \sin \theta_o)$ in (30) and (31). From (32)

$$\overline{E}_z|_{k \rightarrow 0} = -\sin \theta_o$$

$$E_z|_{k \rightarrow 0} = -V/d$$

This corresponds to the average E_z on the source plane.

The amplitude factor can be readily evaluated by the method outlined in Appendix A. As is evident from (35) and (36), for $q = 0$, F_o is independent of d . However, in general, d does affect the values of F_q for $q \neq 0$. We present the following plots of F_o : $b/a = 100$, $\phi_o = 0^\circ$, $\theta_o = 90^\circ, 60^\circ, 45^\circ$, and 30° in Figs.13-16; and $\phi_o = 45^\circ$ and $\theta_o = 90^\circ$ for the same b/a value in Fig.17. It is noticed that the magnitude is considerably larger at lower frequencies. There are frequencies at which F_o vanishes. These correspond to the values when the series in the denominator of F_o is infinite. In the broadside radiation case ($\theta_o = 90^\circ$, $\phi_o = 0^\circ$), this phenomenon is easily identified to be associated with the resonance condition. A careful examination of Figs.13-16 reveals that for a smaller value of θ_o , the value b/λ where F_o first vanishes becomes larger. This provides a technique to broaden the low frequency bandwidth of the array by sloping the source plane with respect to the radiation direction.

In Fig.18, we show the effect of varying ξ for a broadside radiation. Wires with smaller ξ , i.e., thicker wires, have larger $|F_o|$; they are more efficient radiators.

A careful examination of (32), (33), and (35) reveals that there are frequencies at which some field components become infinite. Specifically, these occur when either $\kappa_{pq} = 0$ or $\kappa_q = 1$. The first condition is equivalent to

$$\kappa_{pq} = \sin \theta_q \cos \phi_{pq} = 0$$

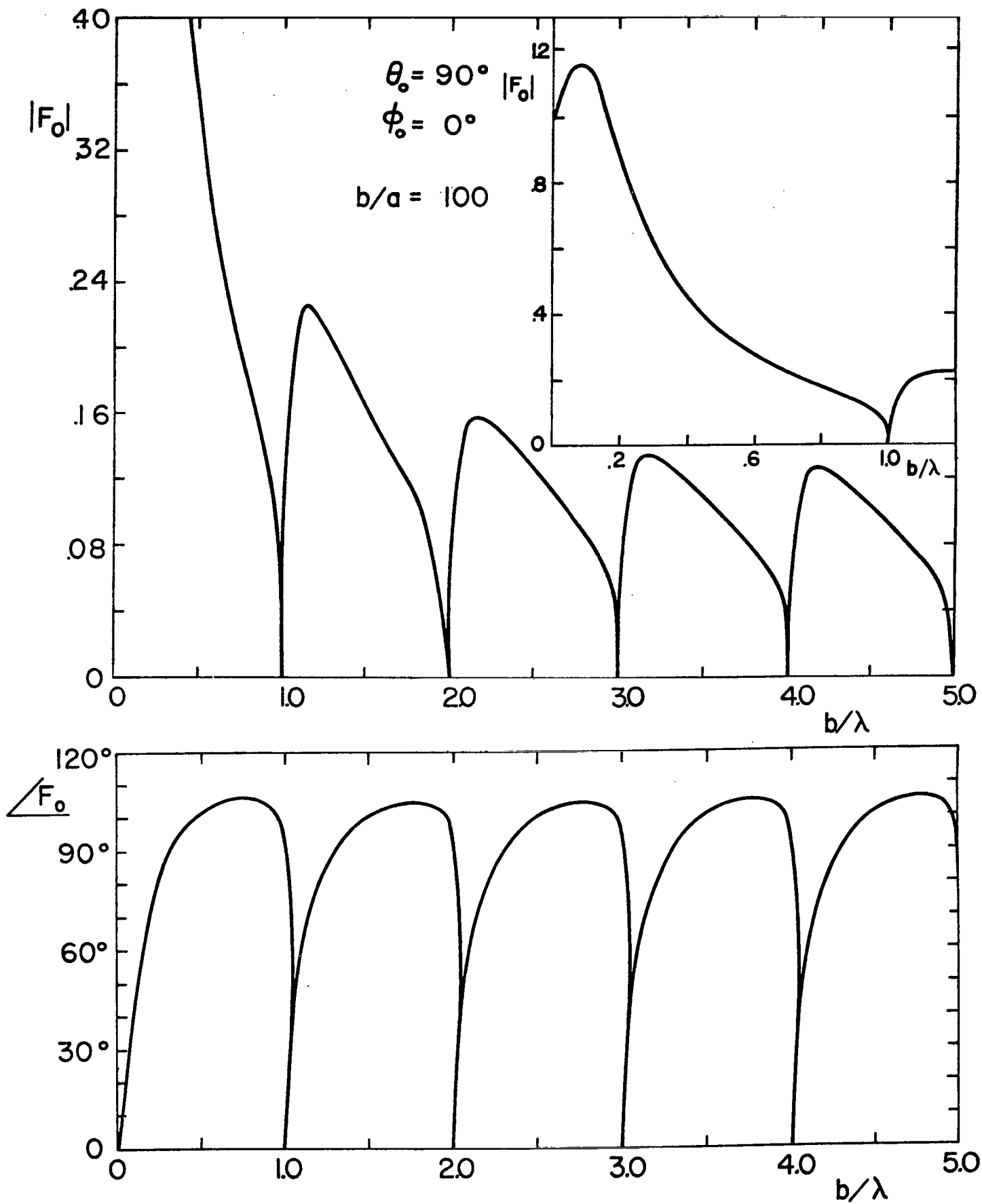


Fig.13. The magnitude and phase of the amplitude factor F_0 . $\theta_0 = 90^\circ$, $\phi_0 = 0^\circ$. F_0 is related to the amplitude of the electric field for the main beam.

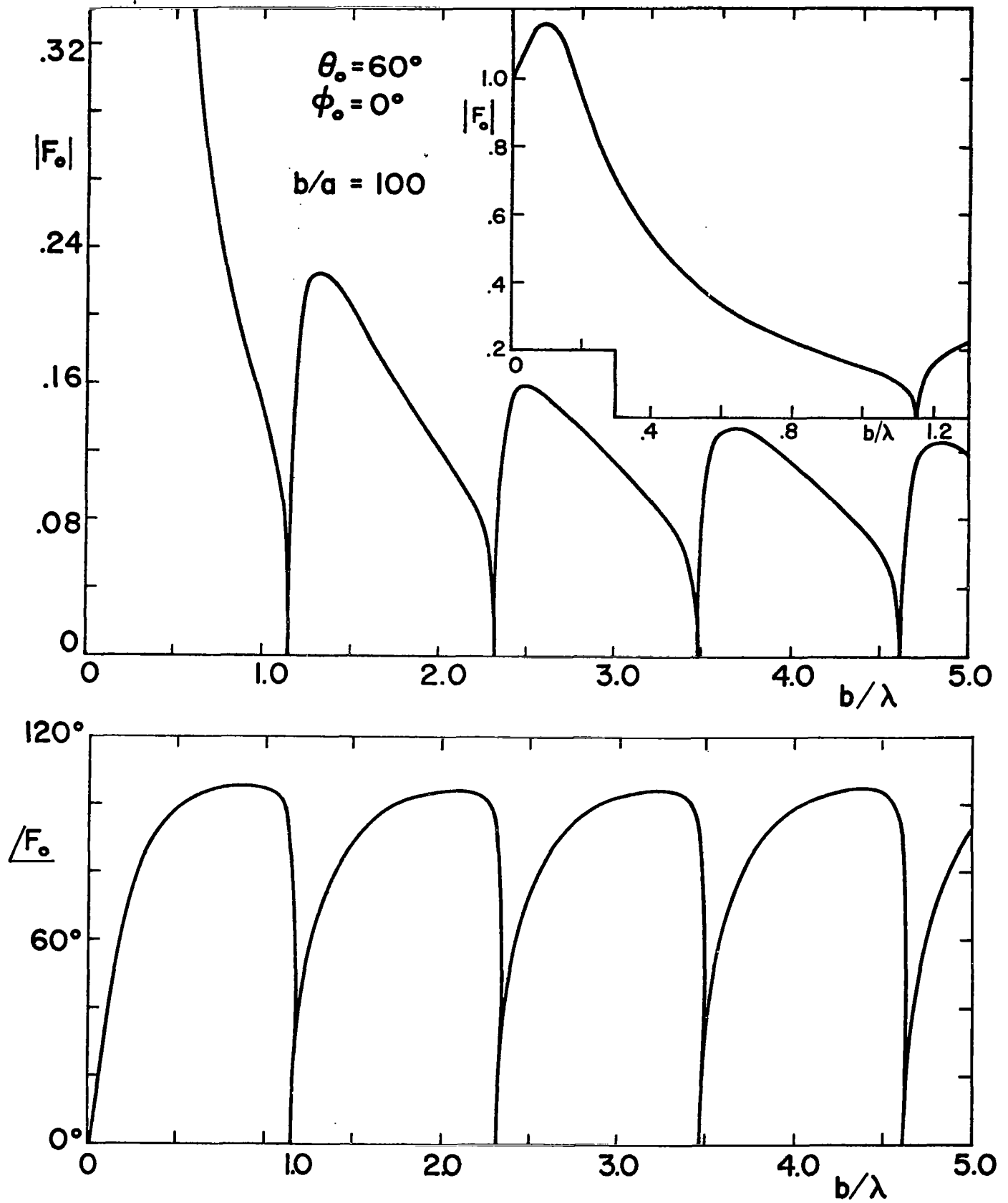


Fig.14. The magnitude and phase of the amplitude factor F_0 . $\theta_0 = 60^\circ$, $\phi_0 = 0^\circ$. F_0 is related to the amplitude of the electric field for the main beam.

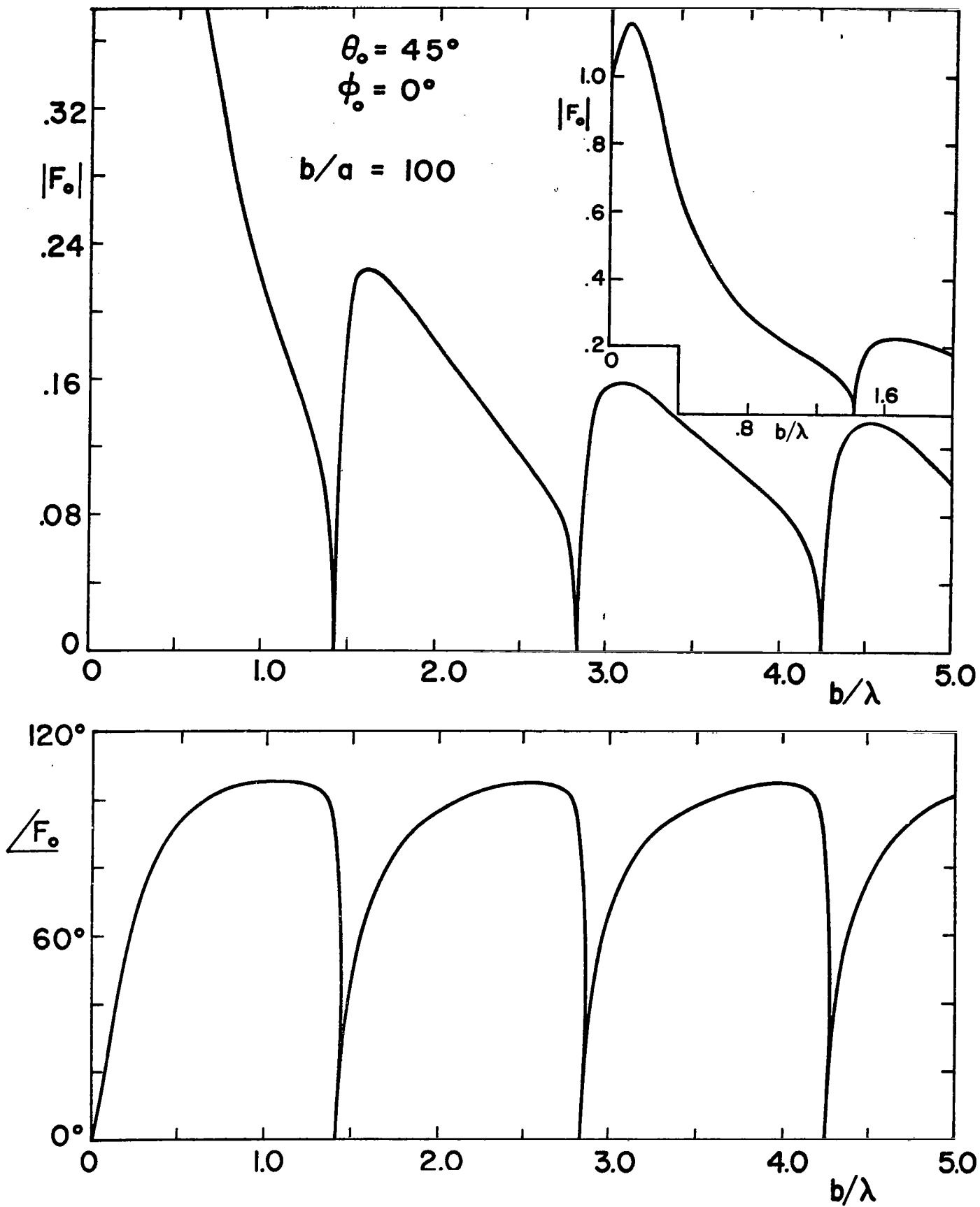


Fig.15. The magnitude and phase of the amplitude factor F_0 . $\theta_0 = 45^\circ$, $\phi_0 = 0^\circ$. F_0 is related to the amplitude of the electric field for the main beam.

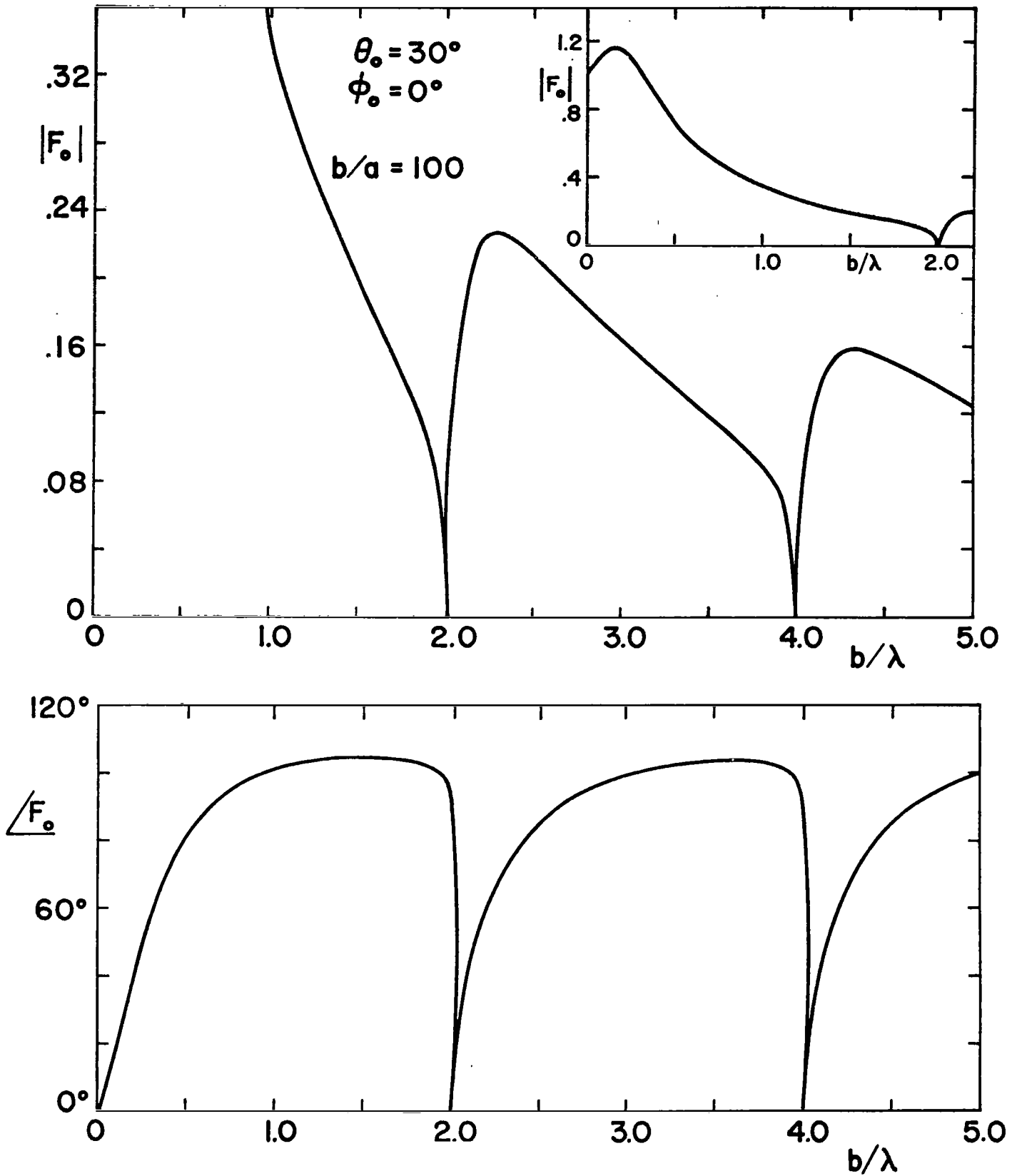


Fig.16. The magnitude and phase of the amplitude factor F_0 . $\theta_0 = 30^\circ$, $\phi_0 = 0^\circ$. F_0 is related to the amplitude of the electric field for the main beam.

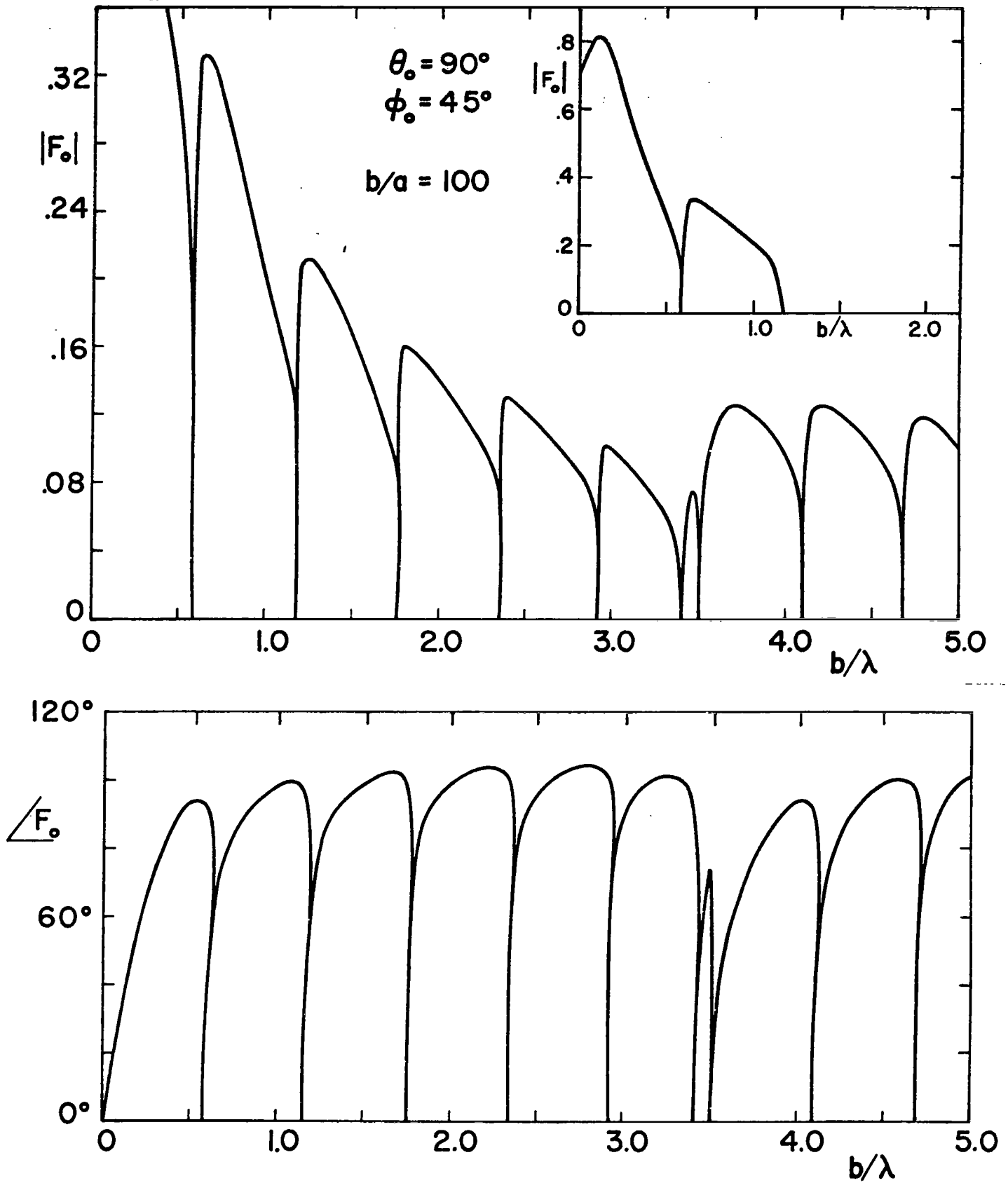


Fig.17. The magnitude and phase of the amplitude factor F_0 . $\theta_0 = 90^\circ$, $\phi_0 = 45^\circ$. F_0 is related to the amplitude of the electric field for the main beam.

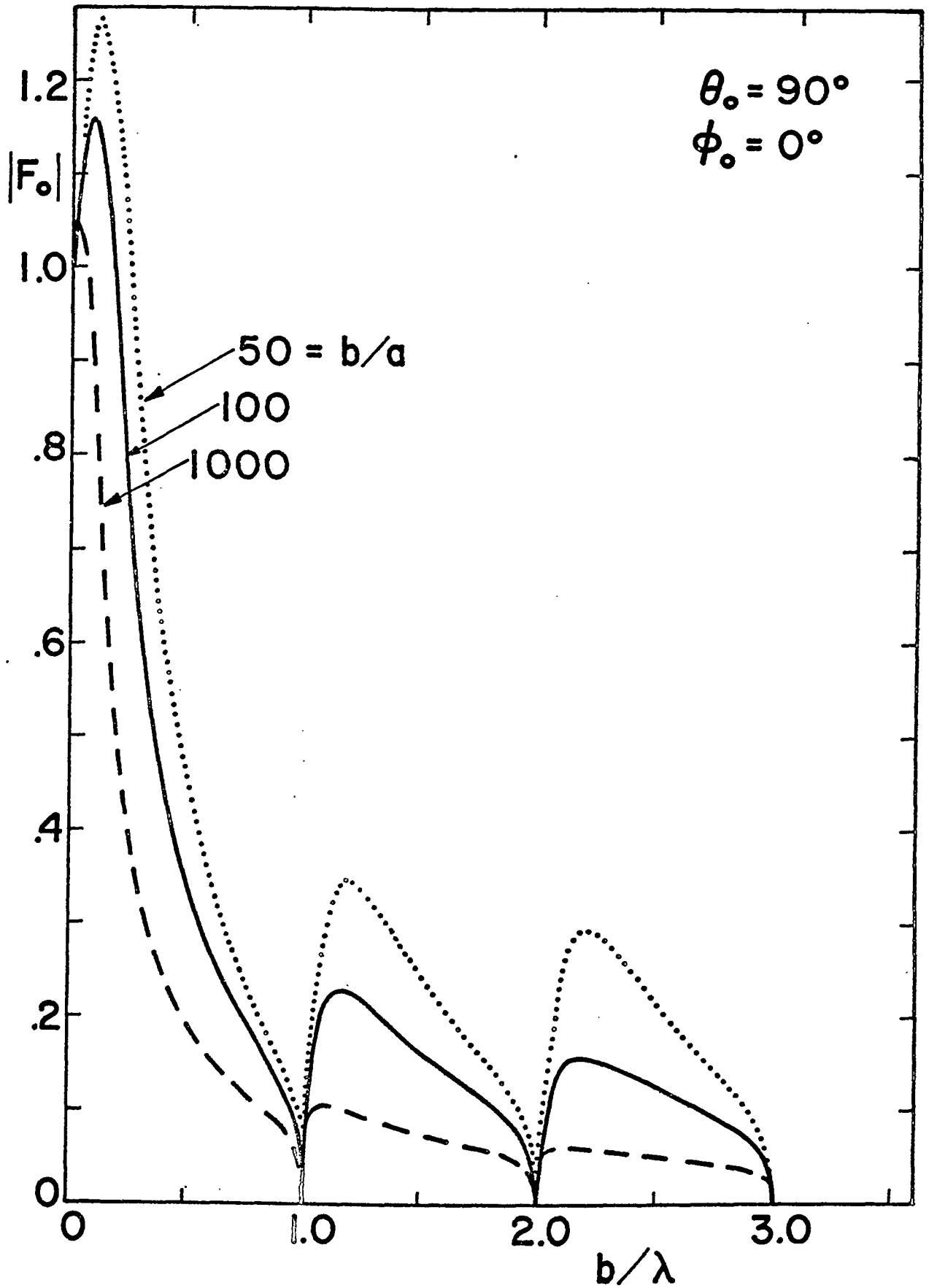


Fig.18. The amplitude factor F_0 for three values of b/d . The thicker antenna is a more efficient radiator.

and the second condition, by (43), is

$$\kappa_q = \cos \theta_q = 1$$

these conditions imply that at the cut-off frequency of a propagating mode, some field components are infinite in the representations of (32) and (33). At the cut-off frequency, the mode is propagating along the source plane. This kind of result is not unusual in this type of modal representation, and at these frequencies, an alternative modal description should be employed [8].

At very high frequency, such that $p\lambda \rightarrow 0$ and $q\lambda \rightarrow 0$, (36) shows that

$$\frac{k}{pq} = \frac{k}{00}$$

and (32) shows that

$$\overline{\underline{E}}_{pq} = \overline{\underline{E}}$$

the total field thus contains many modes propagating in the same direction and with the same amplitude and phase as the main beam, plus contributions from the modes that do not meet the above conditions. It is expected that the field value is very high.

IV. Admittances

In this section, we investigate the driving-point admittances, (which is the same at all source points), and the surface admittances. The latter quantities define the driving requirements of the array in an average sense and is useful at low frequencies.

The current on a wire, as given in (20), is a superposition of many traveling waves. The driving-point admittance at $y = 0$, $z = nd$ is given by

$$Y_{in} = I(z)/V(z) \Big|_{z=nd} = I(z)/(V e^{in\beta z}) \Big|_{z=nd}.$$

From (34), we have

$$\begin{aligned} Z_o Y_{in} &= (2\eta/\sin \theta_o) \sum_{q=-\infty}^{\infty} F_q e^{ik\kappa_q nd - iknd \cos \theta_o} \\ &= (2\eta/\sin \theta_o) \sum_{q=-\infty}^{\infty} F_q = \sum_{q=-\infty}^{\infty} Z_o Y_q \end{aligned} \quad (51)$$

The series in (51) is divergent, giving an infinite admittance value. This is an inherent result of antenna problems with delta gaps. However, the field quantities presented in Section III, remain finite because they are evaluated away from the singular source points. In the following, we outline the steps and review the result of re-deriving (51) for an array with finite source gaps having a uniform gap width w . Assuming a uniform electric field V/w across each gap, (6) becomes

$$\begin{aligned} \left(\frac{\partial^2}{\partial z^2} + k^2 \right) \int_{-\infty}^{\infty} dz' \frac{I(z')}{2\pi a} \sum_{\ell=-\infty}^{\infty} e^{i\ell\beta y} G_{\ell}(\underline{r}; \underline{r}') \\ = i\omega\epsilon_o (V/w) \sum_{n=-\infty}^{\infty} [U(z-nd+w/2) - U(z-nd-w/2)] e^{in\beta z} \end{aligned} \quad (52)$$

where $U(z)$ is the unit step function. After applying Fourier transform (9) to (52), we have

$$(2\pi a)^{-1} (k^2 - \zeta^2)^{-1} \tilde{I}(\zeta) \sum_{\lambda=-\infty}^{\infty} e^{i\lambda\beta_y} \tilde{G}_\lambda(\zeta) = i\omega\epsilon_0 V \frac{\sin(\zeta w/2)}{\zeta w/2} \sum_{n=-\infty}^{\infty} e^{in(\beta_z - \zeta d)} \quad (53)$$

Equation (53) differs from (10) by the factor $\sin(\zeta w/2)/(\zeta w/2)$ on the right hand side. The rest of the derivation is along the same line leading from (11) to (20), with ζ finally replaced by $k\kappa_q$ as in (18) and (19). The driving-point admittance for the finite gap case is

$$Z_0 Y_{in} = (2\eta/\sin \theta_0) \sum_{q=-\infty}^{\infty} \frac{\sin(k\kappa_q w/2)}{(k\kappa_q w/2)} F_q \quad (54)$$

Because of the coefficient $[\sin(k\kappa_q w/2)/(k\kappa_q w/2)]$, the series in (54) now converges. In evaluating (54), the series has to be summed for all values of q , regardless of the condition of κ_{pq}^* . This process is described in Appendix A. We choose to investigate the case of a small gap width, i.e., $k\kappa_q w \ll 1$, and so the effect of the gap width does not appear in the numerical results[†]. For the case of broadside radiation with $\eta = 1$ and $\xi = 100$, the driving-point admittance is presented in Fig.19. At $\kappa_q^2 - 1 = 0$, i.e., at b/λ being integers, the admittance is infinite. This is a phenomenon discussed earlier. The sudden change of admittance at $b/\lambda = \sqrt{2}$ occurs when one of the F_q values ($q = 1$ in this case) vanishes due to the infinite value of the series in F_q . A similar plot for the broadside radiation case with $\eta = 5$ and $\xi = 1000$ is presented in Fig.20.

A quantity of interest is the surface admittance of the source sheet. We define it as the ratio of the average of H_y over a module divided by the average of E_z over the same area, i.e.,

* This is different from the case of wave propagation, where only the terms with κ_{pq} being real are summed.

† Equation (52) can also give the results of the effect of the gap width.

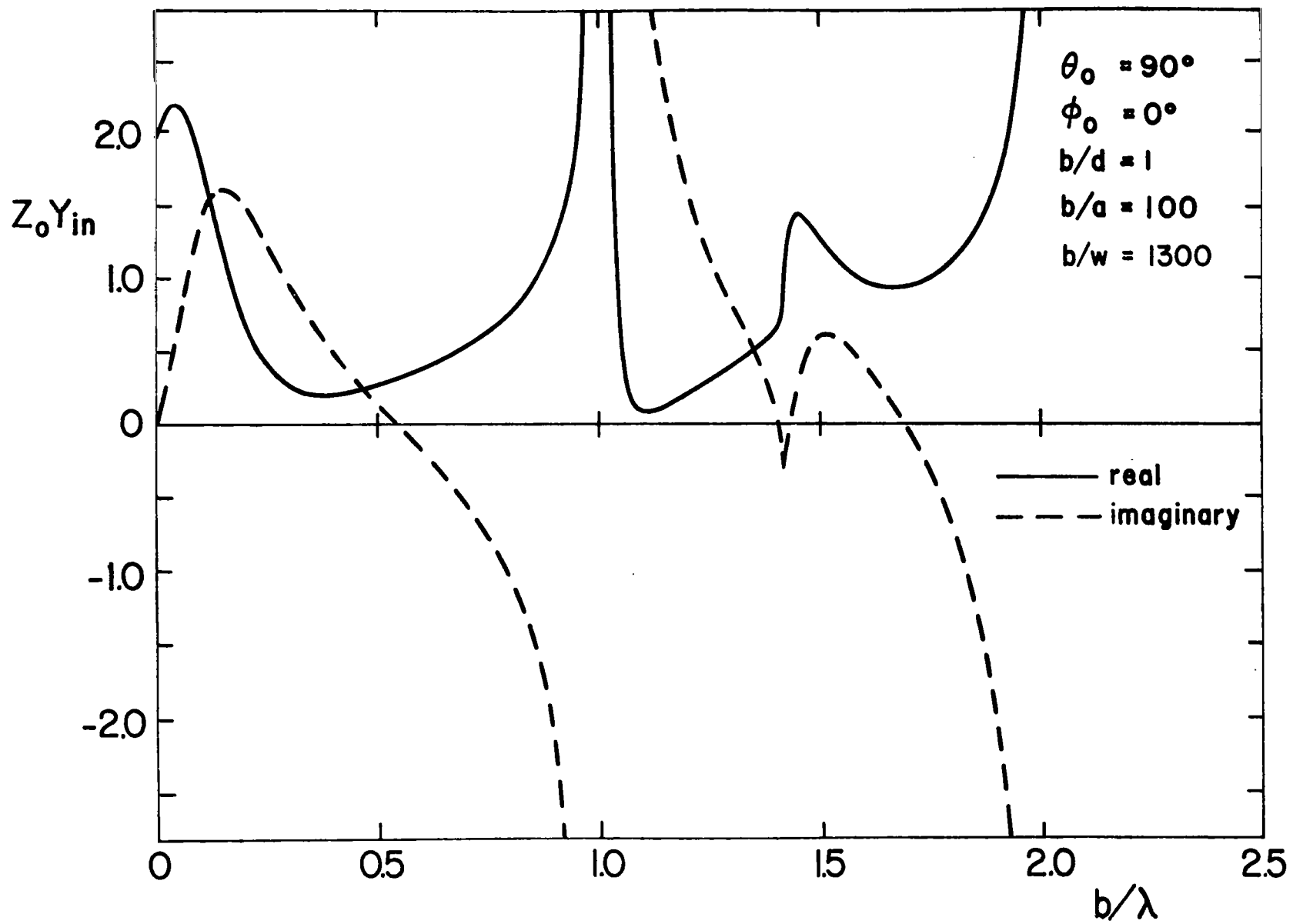


Fig.19. The input admittance as a function of frequency $b/d = 1$, $b/a = 100$, and $b/w = 1300$ where w is the gap width.

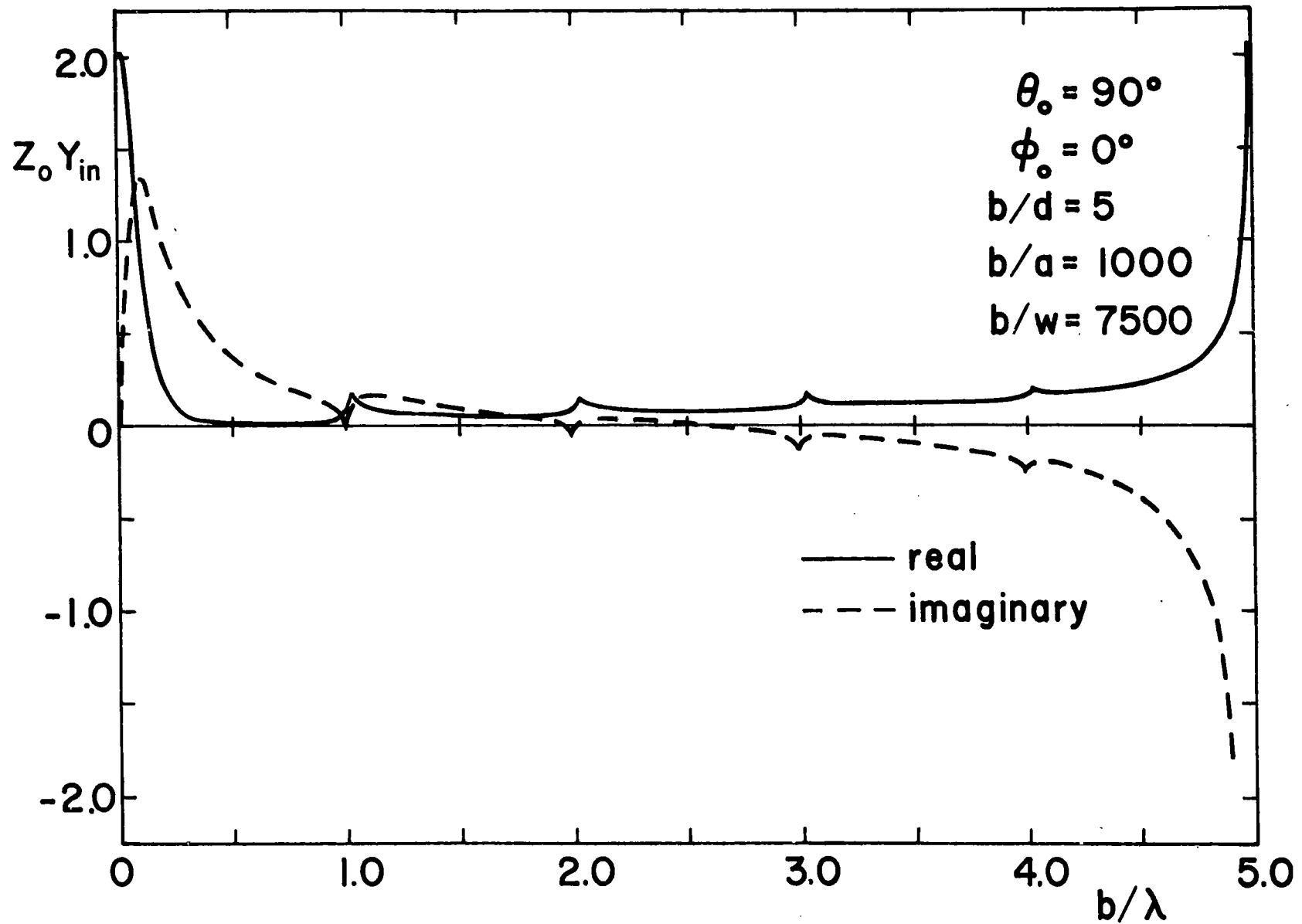


Fig.20. The input admittance as a function of frequency $b/d = 5$, $b/a = 1000$, and $b/w = 7500$ where w is the source gap width.

$$Y_s = - \iint_S \bar{H}_y \, dy \, dz / \iint_S \bar{E}_z \, dy \, dz \quad \text{at } x = 0 \quad (55)$$

where S is the area of one module. This quantity is of particular interest at low frequencies as it defines the admittance of the source array of one side in an average sense. For the low frequency, only the (0,0) mode propagates. Then from (32) and (33), we have

$$Z_o Y_s = (1 - \kappa_q^2|_{q=0}) \kappa_{00}$$

Hence

$$Z_o Y_s = \sin \theta_o / \cos \phi_o$$

For the broadside radiation, $Y_s = + 1/Z_o$. The total average surface admittance of the source array is simply twice the value of Y_s given by (55).

V. Conclusions and Remarks

In the text, we have derived explicit expressions in terms of the E-type modes for a source array excited in a constant-amplitude, progressive-phase fashion. At low frequencies, a TEM plane wave is launched in the desired direction, with amplitude independent of the distance. At higher frequencies, the radiation consists of many TEM plane waves propagating in different directions. It is demonstrated that the propagation directions of the so-called grating lobes change with frequency. The scanning starts at the source plane and ends up in the desired direction. The magnitudes and phases of some field components are calculated. Similar efforts have been carried out for the admittances.

The present work can be expanded into investigating higher frequency behaviors of the fields by carrying out the double summations. The time domain behaviors of the fields and admittances can be examined either by a careful analytical approach or numerical inversion of the frequency domain results. It is also important to investigate the edge effects due to truncating an infinite array into a large but finite one; this corresponds more to the practical case.

Appendix A

Amplitude Factor F_q

In this appendix, we describe the method of evaluating the amplitude factor F_q , which is defined by (35) and re-stated here,

$$F_q = \frac{-i\pi \sin \theta_o}{\xi(\kappa_q^2 - 1)^{\frac{1}{2}}} \cdot K_1 \left(ka \sqrt{\kappa_q^2 - 1} \right) \left\{ K_0 \left(ka \sqrt{\kappa_q^2 - 1} \right) + I_0^{-1} \left(ka \sqrt{\kappa_q^2 - 1} \right) \right. \\ \left. \sum_{\ell \neq 0} e^{i\ell\beta y} K_0 \left(k|\ell|b \sqrt{\kappa_q^2 - 1} \right) \right\}^{-1} \quad (\text{A.1})$$

From (32) and (33), the propagating modes demand

$$\kappa_q^2 - 1 < 0, \quad (\text{A.2})$$

whereas the driving point admittance, as given by (34), does not require this above condition. The method given here is applicable to both cases, provided the proper sign of the square root is taken.

Basically, the problem lies in the series, which has slow convergence. It is possible, however, to transform this into a more convergent series by using the Poisson summation formula. This has been carried out by Wait [13].

Let us denote the series by S_q . Using the Poisson summation formula (16),

we have

$$\begin{aligned}
S_q &= \sum_{\substack{\ell=-\infty \\ \ell \neq 0}}^{\infty} e^{i\ell\beta y} K_0 \left(k|\ell|b\sqrt{\kappa_q^2 - 1} \right) \\
&= \sum_{\ell=-\infty}^{\infty} e^{i\ell\beta y} K_0 \left(k|\ell|b\sqrt{\kappa_q^2 - 1} \right) - \lim_{\ell \rightarrow 0} K_0 \left(\ell kb\sqrt{\kappa_q^2 - 1} \right) \\
&= \sum_{j=-\infty}^{\infty} \int_{-\infty}^{\infty} e^{i\ell\beta y} K_0 \left(k|\ell|b\sqrt{\kappa_q^2 - 1} \right) e^{-i2\pi j\ell} d\ell - \lim_{\ell \rightarrow 0} K_0 \left(\ell kb\sqrt{\kappa_q^2 - 1} \right)
\end{aligned} \tag{A.3}$$

The result so obtained is similar to that of Wait, and is given by

$$\begin{aligned}
S_q &= \ln \left[\frac{1}{2}(b/\lambda)\sqrt{\kappa_q^2 - 1} \right] + \gamma + \frac{1}{2}(b/\lambda)^{-1} \left[\sin^2 \theta_o \sin^2 \phi_o + (\kappa_q^2 - 1) \right]^{-\frac{1}{2}} \\
&+ \frac{1}{2} \sum_{j=1}^{\infty} \left\{ \left[[j-(b/\lambda) \sin \theta_o \sin \phi_o]^2 + (b/\lambda)^2(\kappa_q^2 - 1) \right]^{-\frac{1}{2}} \right. \\
&\quad \left. + \left[[j+(b/\lambda) \sin \theta_o \sin \phi_o]^2 + (b/\lambda)^2(\kappa_q^2 - 1) \right]^{-\frac{1}{2}} - 2/j \right\}
\end{aligned} \tag{A.4}$$

where $\gamma = 0.57721\cdots$ is Euler's constant. The series behaves as j^{-2} for large j , and has relatively fast convergence. It remains to investigate the S_q expression for the propagating modes.

For $\kappa_{q,z}^2 - 1 < 0$, we choose

$$\sqrt{\kappa_q^2 - 1} = -i\sqrt{1 - \kappa_q^2}$$

so that the radiation condition is met. Equation (A.4) now becomes

$$\begin{aligned} S_q = & \ln \left[\frac{1}{2} (b/\lambda) \sqrt{1 - \kappa_q^2} \right] + \gamma + \frac{1}{2} (b/\lambda)^{-1} [\sin^2 \theta_o \sin^2 \phi_o - (1 - \kappa_q^2)]^{-1/2} - i\pi/2 \\ & + \frac{1}{2} \sum_{j=1}^{\infty} \left\{ \left[[j - (b/\lambda) \sin \theta_o \sin \phi_o]^2 - (b/\lambda)^2 (1 - \kappa_q^2) \right]^{-1/2} \right. \\ & \left. + \left[[j + (b/\lambda) \sin \theta_o \sin \phi_o]^2 - (b/\lambda)^2 (1 - \kappa_q^2) \right]^{-1/2} - 2/j \right\} \end{aligned} \quad (A.5)$$

We have to determine the sign when any of the three inverse square roots becomes imaginary. The mathematical reasoning will be given in the later part of this appendix, the result is as follows

$$(f^2 - g^2)^{-1/2} = i(g^2 - f^2)^{-1/2} \quad (A.6)$$

As pointed out in the main text, at low frequency, only the (0,0) mode is propagating. In this case, we can evaluate F_o using (A.5), (A.6) and the small argument expressions for the modified Bessel functions. This asymptotic approximation is equivalent to the use of the thin wire approximation, and mathematically

$$K_0(f) \approx -\ln f$$

$$K_1(f) \approx 1/f$$

and

$$I_0(f) \approx 1$$

From (A.5) and (A.6)

$$\begin{aligned}
 S_0|_{k \rightarrow 0} &= \lim_{k \rightarrow 0} \left[\ln \left[\frac{1}{2}(b/\lambda) \sin \theta_0 \right] + \gamma + \frac{1}{2}i \right] (b/\lambda) \sin \theta_0 \cos \phi_0^{-1} e^{-i\pi/2} \\
 &+ \frac{1}{2} \sum_{j=1}^{\infty} \left\{ \left[[j - (b/\lambda) \sin \theta_0 \sin \phi_0]^2 - [(b/\lambda) \sin \theta_0]^2 \right]^{-1/2} \right. \\
 &\quad \left. + \left[[j + (b/\lambda) \sin \theta_0 \sin \phi_0]^2 - [(b/\lambda) \sin \theta_0]^2 \right]^{-1/2} - 2/j \right\} \\
 &\approx \frac{1}{2} i [(b/\lambda) \sin \theta_0 \cos \phi_0]^{-1}
 \end{aligned}$$

and

$$\begin{aligned}
 F_0|_{k \rightarrow 0} &= \lim_{k \rightarrow 0} \frac{-i\pi \sin \theta_0}{(b/a)(-i \sin \theta_0)} \cdot \frac{1}{ka(-i \sin \theta_0)} \left\{ -\ln(-ika \sin \theta_0) \right. \\
 &\quad \left. + \frac{2i}{(b/\lambda) \sin \theta_0 \cos \phi_0} \right\}^{-1}
 \end{aligned}$$

$$= \cos \phi_0$$

(A.7)

We now return to investigate the sign of the inverse square roots in (A.5). They are the result of the integration in (A.3), and we write

$$I = \int_{-\infty}^{\infty} K_0(|\ell|g') e^{-if\ell} d\ell$$

where, g' corresponds to $kb\sqrt{\kappa_q^2 - 1}$, and f to $2\pi j - \beta_y$.

We now try to evaluate I when

$$g' = -ig$$

where g is positive and real

$$\begin{aligned} I &= \frac{i\pi}{2} \int_{-\infty}^{\infty} H_0^{(1)}(|\ell|g) e^{-if\ell} d\ell \\ &= \frac{i\pi}{2} \left\{ \int_{\ell_1}^{\infty} H_0^{(1)}(\ell g) e^{-if\ell} d\ell + \int_{-\ell_1}^{\ell_1} H_0^{(1)}(|\ell|g) e^{-if\ell} d\ell \right. \\ &\quad \left. + \int_{\ell_1}^{\infty} H_0^{(1)}(\ell g) e^{if\ell} d\ell \right\} \end{aligned}$$

when ℓ_1 is large,

$$H_0^{(1)}(\ell g) \approx \sqrt{2/(\pi\ell g)} e^{i\ell g} e^{-i\pi/4}$$

$$\begin{aligned} I|_{\ell_1 \text{ large}} &\approx \frac{i\pi}{2} \left\{ \sqrt{\frac{2}{\pi g}} e^{-i\pi/4} \left[\int_{\ell_1}^{\infty} \ell^{-1/2} e^{i(g-f)\ell} d\ell + \int_{\ell_1}^{\infty} \ell^{-1/2} e^{i(g+f)\ell} d\ell \right] \right. \\ &\quad \left. + \int_{-\ell_1}^{\ell_1} H_0^{(1)}(|\ell|g) e^{-if\ell} d\ell \right\} \end{aligned}$$

For $g + f$ positive, as required by (A.6), the second integrand is oscillatory and averages to zero. With the knowledge that

$$I \Big|_{g \rightarrow f} \rightarrow \infty$$

and that the third integral is finite, we know that the main contribution of I comes from the first integral, and

$$\begin{aligned} I \Big|_{g \rightarrow f} &\approx i \sqrt{\frac{\pi}{2g}} e^{-i\pi/4} \int_{l_1}^{\infty} l^{-1/2} e^{i(g-f)l} dl \\ &\approx i \sqrt{\frac{\pi}{2g}} e^{-i\pi/4} \int_0^{\infty} l^{-1/2} e^{i(g-f)l} dl \end{aligned}$$

Let us take the case $g - f$ being positive and let

$$\frac{\pi}{2} u^2 = g - f,$$

then,

$$I \Big|_{g \rightarrow f} = i \sqrt{\frac{\pi}{2g}} \frac{1-i}{2} \sqrt{\frac{2\pi}{g-f}} \int_0^{\infty} e^{i\pi u^2/2} du \quad (\text{A.6})$$

This integral is in the form of Fresnel integrals and is readily evaluated [14].

$$I \Big|_{g \rightarrow f} = i\pi [2g(g-f)]^{-1/2}$$

For consistency, we take the positive sign when any of the three inverse square roots are imaginary, i.e.

$$(f^2 - g^2)^{-1/2} = i(g^2 - f^2)^{-1/2}.$$

Acknowledgement

The author thanks Dr. Carl E. Baum for initiating the interest in this work. Valuable suggestions and comments were made by Drs. Kelvin S. H. Lee and Lennart Marin. The manuscript was prepared by Ms. Theresa Abramian.

References

- [1] C. E. Baum, "Some characteristics of planar distributed sources for radiating transient pulses," *Sensor and Simulation Note* 100, March 1970.
- [2] C. E. Baum, "General principles for the design of ATLAS I and II, Part IV: additional considerations for the design of pulser arrays," *Sensor and Simulation Note* 146, March 1972.
- [3] C. E. Baum, "Early time performance at large distances of periodic planar arrays of planar bicones with sources triggered in a plane-wave sequence," *Sensor and Simulation Note* 184, August 1973.
- [4] A. A. Oliner and R. G. Maleck, "Mutual coupling in infinite scanning arrays," in R. C. Hansen (ed.), Microwave Scanning Antennas, vol.II. Academic Press, 1966, Ch.3.
- [5] G. G. MacFarlane, "Surface impedance of an infinite parallel-wire grid at oblique angles of incidence," Journ. IEEE, vol.93, pt.IIIA, pp.1523-1527, 1946.
- [6] J. R. Wait, "Reflection at arbitrary incidence from a parallel wire grid," Appl. Sci. Res., Section B, vol.4, pp.393-400, 1954.
- [7] D. L. Wright, "Sloped parallel resistive rod terminations for two-dimensional parallel-plate transmission lines," *Sensor and Simulation Note* 103, May 1970.
- [8] H. M. Altschuler and L. O. Goldstone, "On network representations of certain obstacles in waveguide region," IRE Trans. on Microwave Theory and Techniques, vol.MTT-7, pp.213-221, April, 1959.
- [9] D. S. Jones, The Theory of Electromagnetism. London: Pergamon Press, 1964.
- [10] E. Hallén, Elektricitetslära. Almqvist & Wiksells, 1953, pp.408-418.
- [11] R. E. Collin, Field Theory of Guided Waves. McGraw Hill, 1960.
- [12] G. A. Campbell and R. M. Foster, Fourier Integrals for Practical Applications. D. Von Nostrand, 1948.
- [13] J. R. Wait, "Reflection from a wire grid parallel to a conducting plane," Canad. J. Phys., vol.32, pp.571-579, September 1954.
- [14] M. Abramowitz and I. A. Stegun (eds.), Handbook of Mathematical Functions, National Bureau of Standards, AMS-55, 1970.